Alma Mater Studiorum – Università di Bologna

Scuola di Scienze
Dipartimento di Fisica e Astronomia
Corso di Laurea magistrale in Astrofisica e Cosmologia

Joint forecasts on primordial fluctuations and neutrino physics from future CMB and galaxy surveys

Tesi di laurea

Presentata da:
Matteo Rossini

Relatore:
Chiar.mo Prof. Lauro Moscardini

Correlatori:
Dott. Fabio Finelli

Dott. Mario Ballardini

Dott. Daniela Paoletti

Sessione III
Anno accademico 2015-2016

Sommario

Il seguente lavoro é incentrato sullo studio delle capacitá del satellite Cosmic Origins Explorer (CORE) di vincolare i parametri che descrivono i modelli cosmologici. CORE é un progetto proposto a Ottobre 2016 per il bando M5 per missioni spaziali di medie dimensioni dell'Agenzia Spaziale Europea (ESA) che si propone di effettuare la survey a tutto cielo ed ad altissima precisione delle anisotropie della radiazione cosmica di fondo a microonde (CMB), con particolare interesse per le anisotropie in polarizzazione, con applicazioni cruciali in cosmologia per quanto riguarda ad esempio lo studio dell'universo primordiale e la fisica dei neutrini. Insieme alle predizioni per il solo CORE si sono derivate anche le predizioni in combinazione con la missione Euclid, attualmente in fase di progettazione, che si occuperá anche di survey spettroscopiche di galassie per lo studio della struttura a grande scala dell'Universo (LSS), con l'obiettivo di verificare il livello di precisione raggiungibile dalla combinazione dei futuri esperimenti CMB e LSS. Come confronto si sono derivate anche le predizioni con la combinazione di Euclid e dell'ultima generazione dei satelliti dedicati all'osservazione della CMB, ovvero Planck, il satellite dell'ESA lanciato nel 2009 che ha completato la presa dati nell'ottobre 2013. L'analisi dei dati simulati é stata svolta tramite l'utilizzo dell'informazione di Fisher, uno strumento statistico che consente di ottenere vincoli sui parametri cosmologici usando un'approssimazione Gaussiana della funzione di likelihood legata ai modelli, con conseguenti formule analitiche che rendono i tempi di calcolo relativamente brevi, soprattutto se comparati a metodi di campionamento come il Markov Chain Monte Carlo

(MCMC), tipicamente usato nelle analisi dati e predizioni per la CMB. A tal proposito si sono confrontati i risultati ottenuti, in particolare quelli relativi allo studio dello spettro delle fluttuazioni primordiali e della fisica dei neutrini, con quelli pubblici degli articoli della Collaborazione CORE, ottenuti appunto con metodi MCMC, in modo da verificare l'affidabilitá delle predizioni ottenute con l'approccio di Fisher. Sono stati studiati il modello cosmologico standard LCDM e alcune sue estensioni, comprendenti i parametri di dipendenza di scala dell'indice spettrale delle fluttuazioni primordiali scalari, chiamati running e running del running dell'indice spettrale, il parametro di curvatura spaziale, il numero di specie relativistiche e la massa totale dei neutrini predette dal modello standard delle particelle. I risultati ottenuti hanno mostrato come le prestazioni di CORE siano nella maggior parte dei casi migliori di quelle date dalla combinazione di Planck e Euclid e come la combinazione di CORE e Euclid consenta di vincolare, in modo molto piú stringente dei valori attuali, gli errori sui parametri cosmologici. Questo grazie anche al fatto che le due missioni si occupano dell'osservazioni di fenomeni, CMB e LSS, dipendenti in maniera diversa dai parametri cosmologici e che quindi le rispettive informazioni possono aiutare a rompere le degenerazioni tra parametri. Per di piú, abbiamo verificato che l'approccio di Fisher riproduce risultati in perfetto accordo con quelli del metodo MCMC nella maggior parte dei casi con ottima precisione.

Contents

Introduction

Cosmology has always been an important branch of physics and astronomy, but for centuries it was only possible to approach to it from a totally theoretical point of view.
The publication of Einstein General Relativity in 1917 put the bases of modern cosmology. In 1929 Edwin Hubble providee the evidence of the expansion of the Universe through the measurements of recession velocities of extragalactic objects obtained from their redshift. This expansion had been already predicted two years earlier from the general relativity equations by Georges Lemaître. This discovery has been the first cosmological observational evidence, as well as one of the most important in support of the Big Bang model.
Afterwards cosmology rapidly became to all intents and purposes a predictive and experimental science, giving results with an increasing accuracy. In the last sixty years, after the discovery of the Cosmic Microwave Background (CMB) radiation, first predicted in 1948 by Ralph Alpher and Robert Herman, and then observed for the first time by chance in 1964 by Arno Penzias and Robert Woodrow Wilson, cosmology advanced with increasingly precise experiments and results. From 1990, thanks to several dramatic tecnological developments in cosmological observations, the Cosmic Background Explorer (COBE), the Wilkinson Microwave Anisotropy Probe (WMAP)and *Planck* satellites gave us more and more accurate data on CMB, large new galaxy redshift surveys including the Two-degree-Field Galaxy Redshift Survey (2dfGRS) and the Sloan Digital Sky Survey (SDSS) provided an incred-

ible amount of data about the clustering of Large Scale Structure (LSS), the gravitational lensing and the distant supernovae.
Next-generation satellites like Euclid, a medium-size space mission currently under development by the European Space Agency (ESA) and telescopes like the Square Kilometer Array (SKA), a large multi radio telescope global project, will begin a new era of high-precision observations, most of which concerning also cosmological topics. Recently the CMB scientic community proposed the Cosmic ORigins Explorer (CORE), a medium-size satellite mission that plans, through a high sensitivity survey of the microwave polarization of the entire sky, to probe cosmic origins, neutrino masses and the origin of stars and magnetic fields, to the M5 ESA call for medium size missions.
This work is focused on the study of the forecast for the CORE proposal, on quantifying the improvements it will have with respect to its predecessor *Planck* and of the potential performances achievable in combination with Euclid mission through joint forecasts of future CMB and galaxy surveys. We have applied a Fisher approach to the forecasts to several extensions of the standardand cosmological model, focusing on the spectral index scale dependences related to the power spectrum of primordial fluctuations, on the spatial curvature density parameter and on neutrino properties, based on different assumption found in literature. The thesis is structured as follows.
In the first chapter we present the basic concepts of the standard Cosmology, giving an overview on the Robertson-Walker metric and the Friedmann-Lematre equations with which we describe the evolution of an homogeneous and isotropic Universe. We review the main aspects of the thermal history of the Universe according to the standard Hot Big Bang model, summarizing the successes and the limits of this model. We introduce the cosmic inflation paradigm as a solution for the problem related to such limits and we describe the basics of its theory. In the end, we present also the parametrization of the ΛCDM model, the current standard model of cosmology.
In the second chapter we give an overview on the cosmological observables that are the object of this work. We describe the CMB and LSS properties,

introducing the tools from the theory of perturbations that are used in order to obtain the angular power spectra of the CMB and the galaxy power spectra.
In the third chapter we introduce the Bayesian approach and the Fisher matrix information that we have adopted in our work. We describe the methodology of our analysis and we discuss the specifications of the surveys included.
In the fourth chapter we present the uncertainties in the cosmological parameters predicted for CORE and the joint forecasts from the combination of CORE and Euclid information about the CMB and LSS observables. We also compare the capabilities of the CORE+Euclid combination with the *Planck*+Euclid one. Furthermore, we check the reliability of the Fisher approach in cosmological parameter estimation with a comparison with a MCMC approach.

Chapter 1

The standard model of Hot Big Bang

One assumption at the base of the standard cosmological model is that the Universe, despite the fact that locally its matter content is clumped into stars, galaxies, and galaxy clusters, is homogeneous and isotropic on large scales. This assumption is known as the Cosmological Principle and basically states that the Universe has the same global properties everywhere, with no preferred position or preferred direction. The anisotropy in the matter distribution observed actualin the local Universe is due to the fact that the litle inhomogeneities in the primordial Universe, during its evolution, grow through the influence of the gravitational force, leading to all the structures we know today.

In this chapter we present the basics of the standard cosmology of the Hot Big Bang model, we describe its main properties and its evolution. We describe the successes and the limits of the model, in order to introduce the cosmic inflation paradigm, its implications and its main results. We thus present the ΛCDM cosmology, the current model that takes into account all the observational evidences of the last decades, like the Cold Dark Matter (CDM) and at late times the Dark Energy (DM), responsible of the new phase of accelerated expansion. For further informations, we refer the reader

to several books and lectures [1, 2, 3, 4].

1.1 The Robertson-Walker metric

In general relativity the line element $\mathrm{d}s$ of a generic coordinate system x^μ at any point in our 4-dimensional spacetime can be written as:

$$\begin{aligned}(\mathrm{d}s)^2 &= g_{\mu\nu}\mathrm{d}x^\mu\mathrm{d}x^\nu \\ &= g_{00}(\mathrm{d}t)^2 + g_{0i}\mathrm{d}x^i\mathrm{d}t + g_{ij}\mathrm{d}x^i\mathrm{d}x^j,\end{aligned} \tag{1.1}$$

where the metric tensor $g_{\mu\nu}$ contains the geometrical information of the space-time in the neighborhood of that local frame and $\mu, \nu = \{0, 1, 2, 3\} = \{t, x, y, z\}$.
The null geodesic condition $g_{00} = c^2$ and the isotropy imply that $g_{0i} = 0$ (no contribution from the mix-terms $\mathrm{d}x^i dt$). If we take into account the homogeneity and the expansion of the Universe, the 3-dimensional line element $(\mathrm{d}l)^2 = g_{ij}\mathrm{d}x^i\mathrm{d}x^j$ can be expressed in spherical coordinates as:

$$(\mathrm{d}l)^2 = a^2(t)\left[\frac{(\mathrm{d}r)^2}{1 - K\,r^2} + S_K^2(r)\left[(\mathrm{d}\theta)^2 + \sin^2\theta\,(\mathrm{d}\phi)^2\right]\right], \tag{1.2}$$

where $a(t)$ is the scale factor of the Universe depending only on the cosmic time t, K is the curvature constant and:

$$S_K(r) = \begin{cases} \frac{\sin(r\sqrt{k})}{\sqrt{k}} & \text{for} \quad k > 0 \quad \text{(closed, spherical Universe)} \\ r & \text{for} \quad k = 0 \quad \text{(flat, euclidean Universe)} \\ \frac{\sinh(r\sqrt{|k|})}{\sqrt{|k|}} & \text{for} \quad k < 0 \quad \text{(open, hyperbolic Universe)} \end{cases} \tag{1.3}$$

The physical distance from us of a given point in the Universe can be written, with a proper choice of coordinate-axis, as $l(t) = a(t)S_K(r)$. The constant (time-indipendent) $S_K(r)$ is called the comoving distance, equal to the physical one at the present time. Comoving coordinates, i.e. coordinates in which observers are moving with the Hubble flow, are often used, as they simplify many calculations. In the same way, one can define the conformal time η

as $\mathrm{d}\eta \equiv \mathrm{d}t/a(t)$ We can thus express the properties of an homogeneous and isotropic space-time with the Robertson-Walker (RW) metric:

$$(\mathrm{d}s)^2 = a^2(t)\left[c^2(\mathrm{d}\eta)^2 - \frac{(\mathrm{d}r)^2}{1 - K\,r^2} + S_K^2(r)(\mathrm{d}\Omega)^2\right]. \tag{1.4}$$

where $(\mathrm{d}\Omega)^2 \equiv \left[(\mathrm{d}\theta)^2 + \sin^2\theta\,(\mathrm{d}\phi)^2\right]$.
At any epoch, the expansion rate of the Universe is given by the Hubble parameter $H(z) \equiv \dot{a}(t)/a(t)$ (the dot represent the time derivative). At present time it is written as $H(t_0) \equiv H_0 = 100\,h\,\mathrm{km\,s^{-1}Mpc^{-1}}$. An other useful quantity is the redshift z due to the expansion of the Universe, defined as $1 + z \equiv \lambda_{\mathrm{obs}}/\lambda_{\mathrm{emit}}$, where λ_{obs} and λ_{emit} are respectively the observed wavelength of a light source and the emission wavelength. The redshift of light at time t is related to the scale factor (from the photon geodesic) by:

$$1 + z = \frac{a(t_0)}{a(t)} = a^{-1}(t), \tag{1.5}$$

where, hereafter, we can consider $a(t_0) = 1$.
Distances in cosmology tend to be measured using redshifts, so the true physical distances are uncertain by a factor h^{-1}, due to the uncertainty on H_0. In order to indicate this, distances are normally given in h^{-1}Mpc units ($1\,\mathrm{pc} = 3.09 \cdot 10^{18}\,\mathrm{cm}$).

1.2 The Friedmann equations

The equations of motion that describes the dynamics of an homogeneous and isotropic Universe are derived from the Einstein field equations:

$$\mathcal{G}_{\mu\nu} = \frac{8\pi G}{c^4} T_{\mu\nu} + \Lambda g_{\mu\nu}, \tag{1.6}$$

where $g_{\mu\nu}$ is the RW metric tensor and $T_{\mu\nu} = -p g_{\mu\nu} + (p + \rho c^2) u_\mu u_\nu$ is the Energy-Momentum tensor for a perfect fluid of 4-velocity u_μ, which takes into account the total energy density ρ of the Universe, the total pressure p (G is the gravitational constant). The second term in the right side of Eq. 1.6 is

the energy contribution of the cosmological constant Λ, an additional energy contribution firstly introduced by A. Einstein as possible explanation of a static Universe, then rejected for the observational evidence of the expansion of the Universe and recently re-introduced after the discovery of its accelerated expansion probed by Supernovae Ia observations at low redshifts.
We start considering the Einstein tensor:

$$\mathcal{G}_{\mu\nu} \equiv R_{\mu\nu} - \frac{1}{2} g_{\mu\nu} R, \tag{1.7}$$

where $R_{\mu\nu}$ is the Ricci tensor and $R \equiv g^{\mu\nu} R_{\mu\nu}$ is the curvature scalar (we assume the Einstein index summation notation). The Ricci tensor can be explicited as:

$$R_{\mu\nu} = \frac{\partial \Gamma^{\lambda}_{\mu\nu}}{\partial x^{\lambda}} - \frac{\partial \Gamma^{\lambda}_{\mu\lambda}}{\partial x^{\nu}} + \Gamma^{\sigma}_{\mu\nu}\Gamma^{\lambda}_{\lambda\sigma} - \Gamma^{\sigma}_{\mu\lambda}\Gamma^{\lambda}_{\nu\sigma}, \tag{1.8}$$

where $\Gamma^{\lambda}_{\mu\nu}$ is the Levi-Civita affine connection. Expliciting it as:

$$\Gamma^{\lambda}_{\alpha\gamma} = \frac{1}{2} g^{\lambda\beta} \left(\frac{\partial g_{\alpha\beta}}{\partial x^{\gamma}} + \frac{\partial g_{\beta\gamma}}{\partial x^{\alpha}} - \frac{\partial g_{\alpha\gamma}}{\partial x^{\beta}} \right), \tag{1.9}$$

we can see how it expresses the effect of the metric tensor on the geometry of the space-time.
Recalling that $dx^{\mu} = \{c\,dt, \mathrm{d}r, d\theta, \varphi\}$, we write the RW metric tensor as:

$$g_{\mu\nu} = \mathrm{diag}\left(1, -\frac{a^2}{1 - Kr^2}, -a^2 r^2, -a^2 r^2 \sin^2\theta\right). \tag{1.10}$$

The non-vanishing terms of the affine connection are:

$$\begin{aligned}
\Gamma^{0}_{\mu\nu} &= \begin{pmatrix} 0 & 0 & 0 & 0 \\ 0 & \Gamma^{0}_{11} & 0 & 0 \\ 0 & 0 & \Gamma^{0}_{22} & 0 \\ 0 & 0 & 0 & \Gamma^{0}_{33} \end{pmatrix}, \qquad
\Gamma^{1}_{\mu\nu} = \begin{pmatrix} 0 & \Gamma^{1}_{01} & 0 & 0 \\ \Gamma^{1}_{10} & \Gamma^{1}_{11} & 0 & 0 \\ 0 & 0 & \Gamma^{1}_{22} & 0 \\ 0 & 0 & 0 & \Gamma^{1}_{33} \end{pmatrix}, \\
\Gamma^{2}_{\mu\nu} &= \begin{pmatrix} 0 & 0 & \Gamma^{2}_{02} & 0 \\ 0 & 0 & \Gamma^{2}_{12} & 0 \\ \Gamma^{2}_{20} & \Gamma^{1}_{21} & 0 & 0 \\ 0 & 0 & 0 & \Gamma^{2}_{33} \end{pmatrix}, \qquad
\Gamma^{3}_{\mu\nu} = \begin{pmatrix} 0 & 0 & 0 & \Gamma^{3}_{03} \\ 0 & 0 & 0 & \Gamma^{3}_{13} \\ 0 & 0 & 0 & \Gamma^{3}_{23} \\ \Gamma^{3}_{30} & \Gamma^{3}_{31} & \Gamma^{3}_{32} & 0 \end{pmatrix}
\end{aligned} \tag{1.11}$$

$$\begin{aligned} &\Gamma^0_{ii} = -\frac{1}{c}\frac{\dot{a}}{a}g_{ii}, \quad \Gamma^1_{11} = -\frac{Kr}{a^2}g_{11}, \quad \Gamma^1_{jj} = -\frac{1}{r}\frac{g_{jj}}{g_{11}} \\ &\Gamma^i_{0i} = \frac{1}{c}\frac{\dot{a}}{a}, \qquad \Gamma^j_{1j} = \frac{1}{r}, \qquad \Gamma^1_{11} = -\sin\theta\cos\theta, \quad \Gamma^3_{23} = \cot\theta, \end{aligned} \tag{1.12}$$

where $\dot{a} \equiv \mathrm{d}a/\mathrm{d}t$. Consequently, we can write the curvature scalar and the non-vanishing term of the Ricci tensor as:

$$\begin{aligned} R_{00} &= -\frac{3}{c^2}\frac{\ddot{a}}{a}, \\ R_{ii} &= -g_{\mu\nu}\left[\frac{2\,K}{a^2} + \frac{1}{c^2}\left(2\frac{\dot{a}^2}{a^2} + \frac{\ddot{a}}{a}\right)\right], \\ R &= -6_{\mu\nu}\left[\frac{2\,K}{a^2} + \frac{1}{c^2}\left(2\frac{\dot{a}^2}{a^2} + \frac{\ddot{a}}{a}\right)\right]. \end{aligned} \tag{1.13}$$

Sobstituing the terms of Eq. 1.13 in Eq. 1.6 we find two indipendent equations of motion that, with respect to the comoving expansion reference frame ($u^0 = c$, $u^i = 0$), can be rearranged as:

$$\frac{\ddot{a}}{a} \equiv \dot{H} + H^2 = \frac{4\pi G}{3}\left(\rho + \frac{3\,p}{c^2}\right) + \frac{\Lambda}{3}, \tag{1.14}$$

and:

$$\left(\frac{\dot{a}}{a}\right)^2 \equiv H^2 = \frac{8\pi G}{3}\rho a^2 - \frac{K}{c^2} + \frac{\Lambda}{3}. \tag{1.15}$$

Eq. 1.14 and Eq. 1.15 are called the Friedmann equations of motion, which describe the evolution of the scale factor and give the expansion rate of the Universe. It is practice to use a conventional notation in cosmology for which $c = 1$ and the gravitational constant G is replaced by the so-called reduced Planck Mass $M_{\mathrm{Pl}} \equiv (8\pi G)^{-1/2} = 2.435 \cdot 10^{18}\mathrm{GeV}$ ($1\,\mathrm{eV} = 1.6 \cdot 10^{-12}\,\mathrm{erg}$).
From the energy conservation law for adiabatic expansion $\mathrm{d}E = -p\mathrm{d}\mathcal{V}$, where $E = \mathcal{V}\,\rho$ is the energy in a comoving volume $\mathcal{V} \propto a^3$, we can derive the continuity equation for fluids, which gives the time dependence of ρ, as:

$$\dot{\rho} = -3\,H(\rho - p) = -3\,H(1 - w)\rho, \tag{1.16}$$

where $w = p/\rho$ is called the parameter of state. The Universe content is assumed to be a gas in almost all its evolution (after Cosmic inflation, as

we will see later, and except during possible phase transitions), so we can assume a mean-square velocity v^2 for each gas component in order to have $w = v^2/3$. For the relativistic component (called radiation) $w \simeq 1/3$ and for the non-relativistic component (called matter) $w \ll 1$. The resulting dependence of energy density from the scale factor is then $\rho_R \propto a^{-4}$ for the radiation (an extra factor a^{-1} comes from the redshift) and $\rho_M \propto a^{-3}$ for the matter (which expresses the mass conservation). Regarding the cosmological constant as a time-independent contribution of the vacuum to the energy density and pressure, we can write $\rho_{\rm tot} = \rho + \rho_\Lambda$ and $p_{\rm tot} = p + p_\Lambda$, with:

$$\rho_\Lambda = -p_\Lambda = M_{\rm Pl}^2 \Lambda, \tag{1.17}$$

i.e., it is constant during expansion (for vacuum pressure, it is thus considered $w = -1$).

For a given value of the Hubble parameter we can see from Eq. 1.15 that it is possible to define the critical density $\rho_c = 3\, M_{\rm Pl}^2 H^2$ for which the Universe (in absence of a cosmological constant) is spatially flat. Its present value is $\rho_{c,0} = 2.775\, h^{-1} \cdot 10^{11} M_\odot/(h^{-1}{\rm Mpc})^{-3}$, where $M_\odot = 1.99 \cdot 10^{33}\,{\rm g}$ is the solar mass. Energy density of the components of the Universe are usually measured as a fraction of ρ_c, defining the density parameters $\Omega_i \equiv \rho_i/\rho_c$ for each component. This includes the contribution of the cosmological constant $\Omega_\Lambda = \Lambda/(3\, H^2)$.

Comparing Eq. 1.15 at t with itself at present time, and considering that $\Omega_i\, H^2 = \Omega_{0,i}\, H_0^2 (1+z)^{3(1+w_i)}$, we can explicite the Hubble parameter at a given redshift with respect to the density parameters dependences, such that:

$$\begin{aligned} H^2(z) &= H_0^2 (1+z)^2 \left(1 - \sum_i \Omega_i + \sum_i \Omega_i (1+z)^{1+3\,w_i)} \right) \\ &= H_0^2 \left[\Omega_{m,0}(1+z)^3 + \Omega_{r,0}(1+z)^4 + \Omega_{\Lambda,0} + (1 - \Omega_{m,0} - \Omega_{r,0} - \Omega_{\Lambda,0})(1+z)^2 \right]. \end{aligned} \tag{1.18}$$

The different scale dependences of the components show that at early times (but well after cosmic inflation), the Universe was radiation dominated.

Since radiation density dropped faster than matter , after the time in which $\Omega_r(z_{\rm eq}) = \Omega_m(z_{\rm eq})$ the matter dominated era begun, where $z_{\rm eq}$ is the redshift of matter-radiation equality, given by:

$$1 + z_{\rm eq} = \frac{\Omega_{m,0}}{\Omega_{r,0}} \simeq 24000\Omega_{m,0}h^2 \tag{1.19}$$

At recent times, $z < 1$, the observations show that Universe has started a period of accelerated expansion. Since the condition for a decelerated expansion is $w > -1/3$ from the Friedmann equations, it was hypotized that we are entered in a period in which Ω_Λ started to dominate over Ω_m. It is usually said that the Universe entered in the Dark Energy (DE) dominated era.

1.3 Thermal history of the Universe

The standard cosmological model is usually named as Hot Big Bang, that assumes a homogeneous, isotropic universe whose evolution is governed by the Friedmann equations. Its main constituents can be described by matter and radiation fluids (at high redshift the presence or not of a cosmological constant is irrelevant).
In this section we give a briefly description of the early stages of the Universe, considering both the assumptions from the Hot Big Bang model and the implications of its extensions that lead to the actual ΛCDM model.

1.3.1 The very early Universe

The term Big Bang was born because, in an expanding Universe, going backward in time it reaches very high (if not infinite in the so-called initial singularity problem associated with classical physics) temperature and densities. We start considering from 10^{-43} sec the Planck epoch, since for smaller times in the standard Big Bang paradigm alternative quantum gravity physics would be necessary. It is only assumed that the temperature was so high ($> 10^{32}$ K) that the four fundamental forces (electromagnetism, weak

interaction, strong interaction and gravitation) were the manifestation of a single fundamental force.
The period $10^{-43}\,\text{sec} \lesssim t \lesssim 10^{-36}\,\text{sec}$ ($10^{30}\,\text{K}$) is called the Grand Unification epoch, in which the expanding Universe cooled and it crossed phase-transition temperatures at which forces separate from each other. This epoch began when gravitation separated from the other forces, described in their unification by a so-called Grand Unified Theory (GUT), and it ended when the GUT forces further separate into the strong and electroweak ones.
At $10^{36}\,\text{sec} \lesssim t \lesssim 10^{-32}\,\text{sec}$ strong force became separated from the electroweak force. The GUT transition at $t \sim 10^{-36}\,\text{sec}$ is supposed to be the beginning of the inflationary period and the electroweak epoch began only at the end of the cosmic inflation, at $t \sim 10^{-32}\,\text{sec}$ ($10^{27}\,\text{K}$). At the end of the inflationary accelerating expansion (that we describe in section 1.4), the ordinary expansion of the Universe began.

1.3.2 The early Universe

After the Cosmic inflation, the Universe entered in the radiation domination era. From this point onwards the physics involved is better understood.
The temperature of the Universe continued to fall during the electroweak epoch $10^{-32}\,\text{sec} \lesssim t \lesssim 10^{-12}\,\text{sec}$. At the end of this period it is supposed that the Higgs field spontaneously acquires a vacuum expectation value, breaking electroweak gauge symmetry. The weak force and electromagnetic force manifest differently in the present universe and, via the Higgs mechanism, all elementary particles interacting with the Higgs field become massive, having been massless at higher energy levels.
The period $10^{-12}\,\text{sec} \lesssim t \lesssim 10^{-6}\,\text{sec}$ ($10^{15}\,\text{K}$) after the electroweak symmetry breaking is called the Quark epoch. The fundamental interactions of gravitation, strong interaction, weak interaction and electromagnetism have taken their present forms and fundamental particles had acquired mass. The Universe is filled with a quarkgluon plasma and the temperature is still too high to allow quarks to bind together to form hadrons.

During the Hadron epoch, at $10^6\,\mathrm{sec} \lesssim t \lesssim 1\,\mathrm{sec}$ ($10^{13}\,\mathrm{K}$) the quarkgluon plasma cools enough to make the color confinement (a phenomenon due to strong interaction) able to clump quarks together into hadrons, including baryons such as protons and neutrons. At $t \lesssim 1\,\mathrm{sec}$ neutrinos decoupled and begun freestreaming through space. Since particles and anti-particles annihilate when their kinetic energy drop below the value of their rest mass energy $T \lesssim m_p$ (we remember $c = 1$), heavier particles annihilate before lighter ones. So, while the majority of hadrons and anti-hadrons started to annihilate each other, leptons (like electron) and anti-leptons begun to dominate the mass of the Universe. The lepton epoch lasted up to $t \lesssim 10\,\mathrm{sec}$ ($10^{10}\,\mathrm{K}$), when also most leptons and anti-leptons are eliminated in annihilation reactions. The fact that we live in a Universe composed by ordinary particles q and we don't observe a relevant amount of anti-particles $\bar{q}$ is called in physics the matter/anti-matter asymmetry problem and still there is not an obvious explanation for why this should be so (but it is a natural assumption that the universe be neutral with all conserved charges). The asymmetry in the number density $(n_q - n_{\bar{q}})/(n_q + n_{\bar{q}}) \sim 10^{-9}$, meaning that for each ordinay particle $\sim 10^9$ pairs has annihilated, producing $\sim 2 \cdot 10^9$ photons. After the annihilation of most leptons and anti-leptons, the energy of the Universe is dominated by photons, still interacting with charged protons and electrons. Between 3 minutes and 20 minutes after the Big Bang, temperature falls to the point where atomic nuclei can begin to form. Free neutrons combine with protons to form deuterium, that rapidly fuses into helium. The formation of primordial Helium, Lithium an Berillium isotopes is called the Big Bang nucleosynthesis, that lasts since the temperature and density of the universe has fallen to the point where nuclear fusion cannot continue. The observation of primordial elements abundances matches quite well with the predictions, making the primordial nucleosynthesis one of the best proofs of the Hot Big Bang model.

At $t \simeq 7{\cdot}10^4\,\mathrm{y}$, the densities of non-relativistic matter and radiation are equal and the matter dominated era begun. DM perturbations start growing under

gravity, while baryonic matter (a conventional name that refers in a general way to hadronic and leptonic ones, since baryons are the dominant component) continues to be coupled with radiation. The tiny inhomogeneities left by cosmic inflation, begun to grow in amplitude, making dense regions denser and rarefied regions more rarefied.

Neutral atoms begin to form as the density of the universe falls, since atom nuclei, previously ionized, begun to capture free electrons. This process is known as recombination. At the end of recombination, at an indicative redshift of $z_{\rm rec} \simeq 1100$ in which half of the Hydrogen atoms become neutral, the photons' mean free path becomes effectively infinite and the photon basically do not interact any more with particles. This cosmic event is usually named decoupling and it is the moment in which the Cosmic Microwave Background (CMB) radiation forms, at $t \simeq 3.77 \cdot 10^5\,\mathrm{y}$, as predicted by the Hot Big Bang model. During the decoupling, overdensity regions attract matter through gravity, but radiation creates an amount of outward pressure. This competition between gravity and pressure created acoustic waves within the electron-baryon plasma, called Baryon Acoustic Oscillations (BAO). When matter becomes completely decoupled, BAO became embedded and frozen in the matter distribution, creating a very little preference in the large scale objects distribution .

Once the baryonic matter decoupled from radiation, it begun to rapidly collapse, following the gravitational potential of the pre-formed clumps of CDM. Analitical models, like the Jeans Theory, or spherical collapse can predict the early phases of structure formation, as long as the theory of perturbation is linear. When we enter in non-linear regime, like the formation of galaxies and cluster of galaxies, analytical models loose reliability and numerical tools become necessary, involving, for instance, N-body simulations with billions of particles.

1.4 Cosmic inflation

The theory of inflation predicts an era of accelerating expansion. In the simplest models it is produced by an hypothetical scalar field called inflaton whose properties should be similar to the Higgs field and some models of dark energy. Inflation theory was developed in the early 1980s, for which the major contributions are the physicists Alan Guth, Andrei Linde and Paul Steinhardt. Nowadays its basic paradigm is accepted by most scientists, since many of its predictions are in agreement with observations.

1.4.1 Unresolved problems in the Hot Big Bang

In the modern view, the most important property of the inflation model is that it naturally explains the generation of the seed of the structures in the Universe, that are primordial fluctuations.
From the historical point of view, the inflation paradigm was created because, despite the great results of the Hot Big Bang model about the primordial nucleosynthesis and CMB predictions, some problems remained within the standard model.
We know from observations that the total density parameter at present time is $\Omega_0 \simeq 1$, implying a flat Universe. We also know from Eq. 1.15 that:

$$\Omega_0 - 1 = \frac{K}{a^2 H^2}. \tag{1.20}$$

Since the combination aH during radiation or matter domination is a decreasing function of time, it means that a nearly flat Universe today implies an extremely flat one in early epochs. For instance, to obtain our present Universe we require at the time of nucleosynthesis ($t_{\rm nuc} \simeq 1\,\text{sec}$) that $|\Omega(t_{\rm nuc}) - 1| \lesssim 10^{-16}$. At earlier time, such as the Planck time ($t_{\rm Pl} \sim 10^{-43}\,\text{sec}$), we should have $|\Omega(t_{\rm Pl}) - 1| \sim 10^{-60}$. Even a small deviation from this flatness would lead to an immediate collapse for closed Universe or to an impressive curvature-dominated expansion for open Universe. The fine-tuning about such unlikely initial conditions is called the flatness problem.

An other issue that the HBB could not explain is the horizon problem. The distance travelled by a photon in a time t represents the maximum causal connection scale achievable in that time, called comoving particle horizon. At the time of CMB formation, at $z_{\rm rec}$, the comoving horizon was roughly 100 Mpc, corresponding to an angle of 1°. One thus would expect, observing two different regions of the last scattering surface [1], that they should have never been in causal contact if they were separated by more than 1°. The CMB pattern show instead a global level of isotropy. The horizon problem also tell us that the large-scale homogeneity and isotropy of the Universe must be part of the initial conditions.
Moreover, the GUT theory predicts unwanted topological defects like magnetic monopoles with both number and energy densities too much high to be compatible with observations.

1.4.2 Basics on inflation

Inflation is defined with a simple statement: any epoch during which the Universe has undergone an accelerated expansion $\ddot{a} > 0$ is an inflationary period. Alternatively, we can give the more physical interpretation in term of the comoving Hubble length $(aH)^{-1}$, that is:

$$\frac{\mathrm{d}}{\mathrm{d}t}\left(\frac{1}{aH}\right) < 0, \tag{1.21}$$

Therefore the condition of inflation is that the comoving Hubble length, which is related to the comoving particle horizon, is decreasing in time, meaning that the observable Universe for an observer become smaller as the inflation proceeds, since the characteristic scale of causal connection reduces in size.
This simple statement immediately resolve all the above mentioned problems. If we compare Eq. 1.28 and Eq. 1.20, we see that inflation implies that Ω is driven toward 1. With a sufficient level of expansion the abundances of

[1] the spherical surface of CMB photons that travels in space from $z_{\rm rec}$ and converges into our position as observers

the monopoles previously created can be reduced enough to be undetectable. Moreover, if the Hubble length is dramatically reduced, it is possible that observed regions that are causally disconnected after inflation was well inside the same particle horizon before the inflation.
The inflaton, in its simplest form, is described by a single, real scalar field. Its Lagrangian density in a generic coordinate system (with the notation $\partial_\mu \equiv \partial/\partial x^\mu$) is:

$$\mathcal{L} = \frac{1}{2} g^{\mu\nu} \partial_\mu \phi \, \partial_\nu \phi - V(\phi), \tag{1.22}$$

where $V(\phi)$ is a function called the potential of the scalar field and the other term is a sort of kinetic term for the field. The energy-momentum tensor of the scalar field is therefore:

$$T_{\mu\nu} = \partial_\mu \phi \, \partial_\nu \phi - g_{\mu\nu} \left(\frac{1}{2} g^{\mu\nu} \partial_\mu \phi \, \partial_\nu \phi - V(\phi) \right). \tag{1.23}$$

In a locally orthonormal frame the momentum density is $T^{0i} = -\dot{\phi} \partial_i \phi$. For spatially homogeneous scalar field $\phi \equiv \phi(t)$, like a perfect fluid, $T^{0i} = 0$, the energy density is $\rho \equiv T^{00}$ and the isotropic pressure is given by $T_{ij} = p \delta_{ij}$, that correspond to:

$$\rho_\phi = \frac{1}{2} \dot{\phi}^2 + V(\phi), \tag{1.24}$$

and:

$$p_\phi = \frac{1}{2} \dot{\phi}^2 - V(\phi), \tag{1.25}$$

where we can note that the scalar field does not possess an equation of state directly relating ρ_ϕ and p_ϕ, because different distribution of the energy density between the potential and the kinetic term can give different values of the pressure for the same ρ_ϕ.
Inserting these two equations into the Friedmann equations, and assuming negligible K and Λ contribution (a reasonable asumption, for the time in which the inflation takes place and for its properties), we obtain:

$$H^2 = \frac{1}{3 M_{\mathrm{Pl}}^2} \left(V(\phi) + \frac{1}{2} \dot{\phi}^2 \right) \tag{1.26}$$

and:

$$\ddot{\phi} + 3\,H\dot{\phi} = -\frac{\mathrm{d}V}{\mathrm{d}\phi} \equiv V'. \tag{1.27}$$

1.4.3 Slow-roll inflation

The simplest models of inflation consider the so-called slow-roll approximation. Defining the slow-roll parameters:

$$\begin{aligned} \epsilon(\phi) &= \frac{M_{\rm pl}^2}{2}\left(\frac{V'}{V}\right)^2, \\ \eta(\phi) &= M_{\rm pl}^2\frac{V''}{V}, \end{aligned} \tag{1.28}$$

we can approximate Eq. 1.26 and Eq. 1.27 respectively as $3\,M_{\rm Pl}^2 H^2 \simeq V(\phi)$ and $3\,H\dot{\phi} \simeq V'$, using the slow-roll conditions $\epsilon(\phi) \ll 1$ and $|\eta(\phi)| \ll 1$.
The slow-roll parameters are a very useful way of quantifying inflationary predictions, as we will show in chapter 4. However, we have to note that even thought they are a necessary condition for slow-roll approximation, they are not a sufficient condition for the inflation. The additional condition is to assume that solutions for the scalar equation has an attractor behaviour. This statement can be sumarized saying that the inflation, in order to be truly predictive, needs that the evolution of the scalar field after some point in the potential has to be independent from the initial conditions. If not, any results would depend on the unknowable initial conditions. The attractor behaviour implies that the differences between solutions of different initial conditions rapidly vanish. With this further condition, slow-roll approximation became a sufficient condition for inflation.
We previously said that inflation is a natural solution for all the above mentioned problems. In order to solve them, we need that the inflationary period lasts enough time. The amount of inflation is normally quantified by the ratio of the scale factor at the end of inflation to its value at some time t as $N(t) \equiv \ln[a(t_{\rm end})/a(t)]$. Since it is typically a large quantity, it is expressed in terms of its logarithm and it is called the number of e-foldings. With the

slow-roll approximation, it can be expressed as:

$$N \equiv \ln\frac{a(t_{\rm end})}{a(t)} = \int_t^{t_{\rm end}} H\mathrm{d}t \simeq \int_{\phi_{\rm end}}^{\phi} \frac{V}{V'}\mathrm{d}\phi. \tag{1.29}$$

To solve the problem mentioned above are usually required (depends on models) around $50-60$ e-foldings of inflation. Furthermore inflation can explain the generation of fluctuations. At quantum level, vacuum fluctuations of the inflaton field $\delta\phi$ are present. During the expansion these fluctuations grows from subatomic scales up to galactic scales and, thanks to their quantum nature, they leads to Gaussian adiabatic density perturbations that are nearly scale-invariant. From the relativistic perturbation theory, one finds that every generic perturbation produced as a consequence of the inflaton field fluctuations (i.e. observables like the CMB anisotropies)is related to the comoving curvature perturbation:

$$\mathcal{R}_k = -\left[\frac{H}{\phi}\delta\phi_k\right]_{t=t_*} \tag{1.30}$$

where k is the spatial frequency in Fourier space and t_* is a reference time. From the power spectrum for the curvature perturbation $P_{\mathcal{R}} \equiv \langle\hat{\mathcal{R}}_k\hat{\mathcal{R}}_{k'}\rangle = |\mathcal{R}_k|^2$. On super-horizon scales the comoving curvature perturbation, and its spectrum, are almost constant. We can thus define a dimensionless power spectrum $\mathcal{P}_{\mathcal{R}}(k) \equiv k^3|\mathcal{R}_k|^2/(2\,\pi^2)$ and evaluate it at horizon crossing $k = aH$, when it is purely a function of k. For this reason, the simplest way to parametrize the primordial power spectrum is:

$$\mathcal{P}_{\mathcal{R}}(k) \equiv A_s\left(\frac{k}{k_*}\right)^{n_s-1}, \tag{1.31}$$

where k_* is a reference scale, n_s is called spectral index and A_s is the amplitude of the primordial spectrum. The exponent $n_s - 1$ takes into account a possible slight deviation from scale-invariance.

1.5 The ΛCDM model

We now present the standard Lambda-Cold Dark Matter model, also called the ΛCDM model. Frequently referred to as the standard cosmological

model, it is the simplest model whose prediction are in good agreement with the observationalproperties of the Universe, such as the CMB anisotropy features, the LSS in galaxy distribution, the abundances of primordial light elements (hydrogen, deuterium, helium, lithium) and the the recent accelerated expansion of the Universe.
As the name suggests, the model includes the effect of dark energy, parametrized with the cosmological constant Λ, and the cold dark matter, the hypothetical form of dark matter whose particles are the main component of the matter density. This implicity mean that the general relativity is assumed as the theory of gravity on cosmological scales and it can be easily extended in order to take into account the cosmological inflation, quintessence and other elements that are current areas of research in cosmology.
The simple ΛCDM model is based on six parameters:

- physical baryon density parameter $\omega_b = \Omega_b h^2$;
- physical dark matter density parameter $\omega_c = \Omega_c h^2$;
- the Hubble parameter at present time H_0;
- the reionization optical depth τ (that we introduce in chapter 2);
- the amplitude of the primordial fluctuation power spectrum A_s;
- the scalar spectral index n_s.

This set of six cosmological parameters is also referred as vanilla ΛCDM. Other details concerning the ΛCDM model and its extensions can be found in next chapters, as part of this work.

Chapter 2

Cosmological observables

The high precision reached in the measurements of the CMB anisotropies in the last decades gave the possibility to constrain the parameters of the ΛCDM model, with an increasing level of accuracy in the field of CMB observations, performed by ground-based and balloon experiments and space missions. An other important source of information is the clustering of the LSS, whose characterisation and contents are studied through sky surveys and spectroscopic mappings.
In this chapter we present the main properties and the information extraction methodology of the CMB anisotropies, which are the dominant source of information about primordial fluctuations, and of the galaxy clustering, whose contribution has a fundamental role in contraining cosmological parameters, even more when combined with CMB measurements. We suggest the following references for further informations [1, 2, 3, 5].

2.1 The Cosmic Microwave Background

The CMB is a nearly isotropic radiation, relic of the Hot Big Bang early phases, with a peak wavelength of $\lambda \simeq 1\,\mathrm{mm}$ and a number density $n_\gamma \simeq 415\,\mathrm{cm}^{-3}$, considered a. It is originated at the recombination,the so-called last scattering surface. Since its photons are originated from scattering

processes that keeps them thermalised with the matter, the CMB shows an exquisite black body spectrum and its temperature is nearly the same, $T_0 = 2.725\,\mathrm{K}$ in all directions. The small anisotropies $\delta T(\hat{n})/T_0 \simeq 10^{-5}$ are the footprints of cosmological matter fluctuations, which seeded the LSS.

2.1.1 Temperature anisotropies

The observed temperature with respect a direction on the sky $\hat{n}$ is:

$$T(\hat{n}) = T_0[1 + \Theta(\hat{n})]. \tag{2.1}$$

We have explicited the contribution of its anisotropies defining the adimensional temperature anisotropy field as:

$$\Theta(\hat{n}) \equiv \frac{\delta T(\hat{n})}{T_0} = \sum_{\ell} \sum_{m=-\ell}^{\ell} a_{\ell m} Y_{\ell m}(\hat{n}), \tag{2.2}$$

where we expand the temperature fluctuation in spherical harmonics $Y_{\ell m}$ and with the multipole moments $a_{\ell m}$ defined as:

$$a_{\ell m} = \int \mathrm{d}\Omega Y^*_{\ell m}(\hat{n})\Theta(\hat{n}) \tag{2.3}$$

where $\mathrm{d}\Omega$ is the solid angle element.

The dominant temperature anisotropy is due to our relative motion (from the Earth up to the Milky Way contributions) with respect to the CMB reference frame, that generates anisotropies in the dipole moment $\ell = 1$. The observations have the dipole removed in order to investigate cosmological anisotropies.

Assuming rotational invariance from the cosmological principle, the variance of the multipole moments is related to the angular power spectrum through:

$$\langle a^*_{\ell m} a_{\ell' m'} \rangle = \delta_{\ell \ell'} \delta_{m m'} C_\ell, \tag{2.4}$$

where the angle brackets denotes an average of the fluctuations over an ensamble of realizations. A noise-free measurement of the temperature fluctuations would give an estimation of the CMB angular power spectrum as.

$$\hat{C}_\ell = \frac{1}{2\ell + 1} \sum_{m=-\ell}^{\ell} |a_{\ell m}|^2 \tag{2.5}$$

where the true ensemble C_ℓ is related with the unbasied estimator $\hat{C}_\ell$ by an irremovable statistical uncertainty called cosmic variance due to the finite number of independent modes $(2\ell + 1)$.
The relation between the primordial power spectrum $\mathcal{P}_\mathcal{R}$ and the temperature fluctuation is given by:

$$a_{\ell m} = 4\pi(-i)^\ell \int \frac{\mathrm{d}^3k}{(2\pi)^3}\, \Theta_\ell(k)\, \mathcal{P}_\mathcal{R}(k) Y_{\ell m}(k), \tag{2.6}$$

where $\Theta_\ell(k)$ is a transfer function that takes into account all the effects that influnce the original form of the primordial fluctuations and, as consequence, of the temperature fluctuations. The expression for C_ℓ in terms of this transfer function is:

$$C_\ell = \frac{2}{\pi} \int k^2 \mathrm{d}k\, \mathcal{P}_\mathcal{R}(k)\, \Theta_\ell^2(k). \tag{2.7}$$

The effects accounted in this way are those that originate the temperature anisotropies, which are divided in primary anisotropies (originated at the formation of the CMB at z_{ls}) and secondary anisotropies (caused by later times at $z < z_{\mathrm{ls}}$).
When the photons are emitted, the gravitional potential of the DM wells induces a redshift of the photons whereas if they are emitted in a sub-dense region, they are blue-shifted. On the other hand, over-dense regions have adiabatic fluctuations that make the photon temperature higher. Both effect are related to the density fluctuations, and their sum, called the Sachs-Wolfe (SW) effect, has the result $\delta T =$
$phi/3$, where ϕ represent the gravitational potential fluctuation (i.e. hotter regions in CMB temperature maps correspond to sub-dense regions of the DM density ditribution). Moreover, the proper motion of the source at the emission contributes to an additional Doppler shift.
During their travel from the surface of last scattering up to us, CMB photons are subjected to different phenomena. During the evolution of the Universe different effects produce variations in the global gravitational potential that in turn influence the CMB photons. This effect is called Integrated SW

(ISW). Although the CMB is produced during the matter domination era, the presence of the radiation density is still relevant at $z \lesssim z_{\rm ls}$. This produces a decrease of the gravitational potential. We refer to this contribution as the early-ISW. The analogous situation occurs during the transition from matter to DE domination era and the anisotropies produced by this variations of the gravitational potential are referred to the late-ISW effect. Moreover, the non-linear evolution of structures produces rapid changes in their gravitational wells. For this reason a photon interacting with the potential of such structures is affected by different shifts in its energy at the beginning and at the end of the interaction (Rees-Sciama effect). Other source of secondary anisotropies are the gravitational lensing effect of the structures on the CMB photon path, that produces an acromatic defletion (temperature does not change, but photon distribution is distorted), and the hot gas in galaxy clusters, which transfer energy to the CMB through inverse Compton scattering, distorting the CMB spectrum (Sunyaev-Zel'dovich effect).
The last but fundamental phenomenon we mention is the reionization. After the formation of the first stars the Universe began to reionize, and free electron could re-scatter CMB photons, smoothing the CMB peaks. The visibility function at reionization is therefore not perfectly sharp and the anisotropies get suppressed as $\Theta e^{-\tau}$, where τ is the reionization optical depth.

2.1.2 CMB polarization

Linear polarization is produced during recombination through Thompson scattering processes between CMB photons and free electrons. Polarized specific brightness of photons with frequency ν is formally described in terms of Stokes parameters, i.e. the total intensity $I(\bar{n}, \nu)$, the difference in brightness between two orthogonal linear polarizations $Q(\bar{n}, \nu)$, the difference in brightness $U(\bar{n}, \nu)$ between two linear polarization at $45^{\odot}$ to those used for defining Q, and the circular polarization $V(\bar{n}, \nu)$. The primordial circular polarization is expected to be null, since Thompson scattering of the CMB does not generate it.

The total intensity I correspond to the temperature , therefore its anisotropy field can be expandend in terms of scalar spherical harmonics, being invariant under rotation in the plane perpendicular to $\hat{n}$, as in Eq. (2.2). The quantities Q and U instead trasform under rotation as a spinor field and their expansion is done in terms of tensor spherical harmonics:

$$(Q \pm iU)(\hat{n}) = \sum_{\ell} \sum_{m=-\ell}^{\ell} a_{\ell m}^{(\pm 2)} Y_{\ell m}^{(\pm 2)}(\hat{n}), \tag{2.8}$$

where $Y_{\ell m}^{(\pm 2)}(\hat{n})$ are spin-± 2 spherical harmonics. In CMB literature, instead of the momenta $a_{\ell m}^{(\pm 2)}$ and the Stokes parameter Q and U, it is used to introduce:

$$\begin{aligned} a_{\ell m}^{E} &\equiv -\frac{1}{2}\left(a_{\ell m}^{(+2)} + a_{\ell m}^{(-2)}\right), \\ a_{\ell m}^{B} &\equiv -\frac{1}{2\,i}\left(a_{\ell m}^{(+2)} - a_{\ell m}^{(-2)}\right), \end{aligned} \tag{2.9}$$

in order to get the adimensional polarization anisotropy fields:

$$\begin{aligned} E(\hat{n}) &= \sum_{\ell} \sum_{m=-\ell}^{\ell} a_{\ell m}^{E} Y_{\ell m}(\hat{n}), \\ B(\hat{n}) &= \sum_{\ell} \sum_{m=-\ell}^{\ell} a_{\ell m}^{B} Y_{\ell m}(\hat{n}). \end{aligned} \tag{2.10}$$

E-mode is a curl-free polarization whose polarization vectors are radial around cold spots and tangential around hot spots in temperature maps. B-mode polarization is divergence-free and its vectors produce vortics around any spot.

The generalization of the angular power spectra can be defined now as:

$$\hat{C}_{\ell}^{X} \equiv \frac{1}{2\ell+1} \sum_{m=-\ell}^{\ell} \langle a^{x*}{}_{\ell m} a_{\ell m}^{x'} \rangle, \tag{2.11}$$

where $x, x' = \{T, E, B\}$ and X denote the four types of correlation between temperature and polarization anisotropies, i.e. three autocorrelations denoted as TT, EE and BB plus the cross-correlation between temperature

and E-mode ones, denoted as TE. Cross-correlation terms with B-mode polarization, TB and EB , vanish under parity symmetry conservation. Furthermore, primordial B-mode polarization is not produced by scalar perturbations in linear perturbation theory (observed B-modes are due to the weak lensing that partially deflect the E-mode signal), while tensor perturbations, the primordial gravitational waves, could produce both E- and B-modes.

2.1.3 CMB weak lensing

The matter density field between the last scattering surface and us produces weak lensing distorsions in the CMB maps, characterized by a deflection field $d(\hat{n})$ which maps the total shift in the direction of a photon path from $z_{\rm rec}$, giving:

$$\widetilde{\Theta}(\hat{n}) = \Theta(\hat{n} + d(\hat{n})) \tag{2.12}$$

and:

$$(\widetilde{Q} \pm i\widetilde{U})(\hat{n}) = (Q \pm iU)(\hat{n} + d(\hat{n})), \tag{2.13}$$

where the lensed fields are denoted with a tilde. The deflection field can be written, at leading order, as the gradient of the lensing potential $d(\hat{n}) = \nabla\phi(\hat{n})$. Expanding in spherical harmonics the lensing potential map, we obtain:

$$\begin{aligned} \phi(\hat{n}) &= 2\int_0^{z_{\rm rec}} \frac{{\rm d}z}{H(z)} \left(\frac{1}{\chi(z)} - \frac{1}{\chi(z_{\rm rec})}\right) \Phi(\hat{n}, z) \\ &= \sum_\ell \sum_{m=-\ell}^{\ell} a^\phi_{\ell m} Y_{\ell m}(\hat{n}) \end{aligned} \tag{2.14}$$

where $\chi = S_K(r)$ is the comoving distance and Φ is the gravitational potential of the density field crossed by CMB photons in $\hat{n}$ (the first equality shows that lensing potential is the 2D-projection in the sky of Φ). For the expansion of the deflection angle map, one just have to consider that:

$$a^{\rm d}_{\ell m} = -i\sqrt{\ell(\ell+1)}\, a^\phi_{\ell m}. \tag{2.15}$$

and the corresponding (autocorrelation) angular power spectra are related by:

$$C_\ell^{dd} = \langle a^{d*}_{\ell m} a^d_{\ell m} \rangle = \ell(\ell+1) C_\ell^{\phi\phi}. \tag{2.16}$$

2.2 The galaxy clustering

Once it becomes decoupled from radiation, baryonic matter density perturbations above the Jeans scale[1], grow following the gravitational wells of the already formed DM structures, originated from matter fluctuations produced by the perturbations on the metric after the inflationary period. Those that are below this scale instead start to oscillate as a standing way, because of the competition of gravity and internal pressure. This phenomenon is called Baryon Acoustic Oscillation (BAO), which is of fundamental importance because its features are direcly observable in CMB and galaxy power spectra. The best observable for testing theories of structure formation is the galaxy clustering, since their distribution is strongly influenced by the presence of DM overdense regions. Unfortunately, galaxies are not perfect tracers of the DM distribution. It is used to say that they are biased tracers, meaning that galaxy distribution does not determine the DM distribution. Furthermore, the level of this bias depends on redshift and it varies for different types of galaxies.

2.2.1 Matter perturbations

Density perturbation and metric fluctuations are related by the Einstein field equations from the relativistic perturbation theory. Matter density perturbations are usually defined as:

$$\delta_m \equiv \frac{\delta\rho_m}{\rho_m}. \tag{2.17}$$

[1] Jeans scale characterizes the limit over which a self-gravitating gas collapse for the impossibility of its internal pressure to counterbalance gravity

The Newtonian potential at low redshift in Fourier space can be written as:

$$\Phi(k,a) = \frac{9}{10}\Phi_0(k)T(k)D(a), \tag{2.18}$$

where $T(k)$ is a transfer function that takes into account micro-physics effects for those wavelength that crosses the Hubble radius and the effect of the transition from radiation to matter domination and $D(a)$ is the growth factor, that gives the relative size of δ_m as function of the scale factor (or, equivalently, the time).
Density perturbation in DM can be related, on small scales, to the gravitational potential through the Poisson equation, which in Fourier space is:

$$4\pi G\rho_m a^2\delta_m = -k^2\Phi(k,a). \tag{2.19}$$

and we thus get:

$$\delta(k,a) = \frac{3}{5}\frac{k^2}{\Omega_m H_0^2}\Phi_0(k)T(k)D(a). \tag{2.20}$$

What we actually observe today related to the matter density perturbations δ_m is their isotropic two-point correlation function or, equivalently, their Fourier transform matter power spectrum, since:

$$\langle\delta_m(k,a)\delta_m^*(k',a)\rangle = (2\pi)^3\delta_{\rm D}^{(3)}(k-k')P_m(k). \tag{2.21}$$

Therefore, assuming a primordial power spectrum as in Eq. (1.31) and since in conformal Newtonian gauge we have, after inflation, $\mathcal{R} = 3\Phi/2$ (thus $P_\mathcal{R} = 9P_\Phi/4$), the DM dimensionless power spectrum on small scales is:

$$\mathcal{P}_m(k) = \frac{4}{25}\frac{A_s}{\Omega_m H_0^2}\left(\frac{k}{k_*}\right)^{n_s+3}T^2(k)D^2(a) \tag{2.22}$$

We have mentioned above that the invisible DM distribution can be traced with galaxy observations, which make possible to estimate the matter and the primordial power spectra, only taking ino account that they are biased tracers. This can be done with a multiplicative factor b, called linear bias, for which:

$$\delta_g \simeq b\,\delta_m. \tag{2.23}$$

However, other effects have to be considered in order to modelling the galaxy redshift-space power spectrum. For other details, we refer to section 1.3.3, where we describe our analysis of spectroscopic galaxy surveys.

Chapter 3

Statistical framework and experimental setup

The statistical inference plays a fundamental role in the achievement of an high level of accuracy in the analysis of the data from CMB and LSS observations. Thanks to development of simulation tools, we are also able to analize mock data generated with simulations to perform forecasts from future experiments.
In this chapter we introduce the Bayesian inference, that is the statistical approach we follow in our work, and the Fisher information, a statistical tecnique that we have adopted in order to provide the forecasts from the mock data of the simulated CMB and LSS surveys. We also describe the methodology of our analysis and the inclusion of survey specifications.

3.1 Bayesian statistics

The two main approaches to statistical analysis are the frequentist and the Bayesian inference, differing in the interpretation of the concept of probability. Frequentists define the probability as the number of times an event occurs divided by the total number of events in the limit of an infinite series of equiprobable trials. The Bayesian approach instead defines the probabil-

ity as the degree of belief in a hypotesis, to evaluate which it is possible to specify some prior probability, depending on the knowledge owned about the hypotesis, that is then updated to a posterior probability thanks to the data, or evidence, available.
We adopt the Bayesian approach, widely used in cosmology, and we now itroduce its basic concepts.

3.1.1 Bayes' theorem

We now introduce more precisely the concepts of Bayesian statistics. Given two arbitrary events A and B, the conditional probability $P(A|B)$ can be written as the ratio between their joint probability and the probability of B (Kolmogorov's definition):

$$P(A|B) = \frac{P(A \cap B)}{P(B)}, \tag{3.1}$$

It is possible to define $P(B|A)$ in the same manner, and so we have that:

$$P(A|B)P(B) = P(A \cap B) = P(B|A)P(A). \tag{3.2}$$

We can write, making explicit with respect to $P(A|B)$ when $P(B) > 0$, the simplest form of the Bayes' Theorem (from Thomas Bayes, 1763 [6]), on which all the Bayesian inference is based:

$$P(A|B) = \frac{P(B|A)P(A)}{P(B)}. \tag{3.3}$$

If we think about A and B in Eq. (3.3) respectively as the hypotesis, or model, M that we want to study and the data D that we have collected, the Bayesian definition of probability tells us that the posterior probability $P(M|D)$ after the occurrence of D is equal to the likelihood $P(D|M) \equiv \mathcal{L}$ of the model multiplied by some prior function $P(M)$, which represents our knowledge about the phenomenon we analyse. The terms $P(D)$ at the denominator is the evidence, acting as a normalization factor.

3.1.2 Parameter estimation

A model M is generally written in terms of an ensemble of parameters $\theta = \{\theta_n\}$ and we want to find the set which best fits the data. The simplest way to do this is the method of the least square:

$$\chi^2 = \sum_i w_i \left[D_i - y(x_i \mid \theta)\right]^2, \tag{3.4}$$

where D_i is a set of data points, $y(x \mid \theta)$ is the theoretical model and w_i are suitably defined weights. If the data are correlated and we choose $w_i = \sigma_i^{-2}$, where σ_i is the error on data point i, the Eq. (3.4) becomes the chi-square, equal to:

$$\chi^2 = \sum_{ij} \left[D_i - y(x_i \mid \theta)\right] \mathcal{C}_{ij}^{-1} \left[D_j - y(x_j \mid \theta)\right], \tag{3.5}$$

where $\mathcal{C}_{ij} = \langle (D_i - y_i)(D_j - y_j) \rangle$ is the covariance matrix. If the data have a Gaussian distribution, we can write the likelihood $\mathcal{L} \propto \exp(-\chi^2/2)$ like a multi-variate Gaussian:

$$\mathcal{L} = \frac{1}{(2\pi)^{n/2}|\mathcal{C}|^{1/2}} \exp\left[-\frac{1}{2}\sum_{ij}(D-y)_i \mathcal{C}_{ij}^{-1}(D-y)_j\right], \tag{3.6}$$

The χ^2 is minimized by the best-fit parameters and corresponds to maximize the likelihood. It can be noticed that the relative probabilities of the parameters do not depend on $P(D)$. The prior distribution instead can be based on previous experiments or it can be a theoretical prior. A possibility is the principle of indifference, that consists in assuming that all the parameters are equally likely in the parameter space, i.e. taking $P(M)$ constant everywhere and referring to it as a flat prior.

In general the choice of the prior could influence the resulting posterior distribution and one has to justify each deviation from the flat prior, considering physical reasons about the parameters or models.

Under these assumptions, it is possible to write the posterior distribution in terms of the single likelihood:

$$P(M|x) \propto \mathcal{L}(x, \theta), \tag{3.7}$$

with which, using the peak of the distribution, it is possible to estimate the parameters.
All these considerations are based on the assumption of a Gaussian likelihood. In case of not Gaussianly distributed data it can be shown that, for the central limit theorem, it is possible to bin the data so that in each bin there is a super-position of many independent measurements [9]. In this way the resulting error distribution for each bin can be approximated by a multi-variate Gaussian. Anyway, even with Gaussian-distributed data, the likelihood function could deviate from a multi-variate Gaussian and so one has to be sure, to avoid this, that the model has a linearly dependence on the parameters.

3.2 Fisher information

Let us assume that we want to measure the amount of information carried by an observable random variable x about unknown parameters θ_i of its distribution. One of the best tools used in Bayesian statistics is the Fisher information: the variance of the expected value, or score, of the observed information.
The first person to emphasize the importance of the Fisher information in the theory of maximum-likelihood estimation was the statistician Ronald Fisher [10], showing that the posterior distribution, usually dependent on the prior, in its asymptotic-limit case is related only to the Fisher information.

3.2.1 Gaussian approximation of the likelihood

First of all, we have to see how to obtain the error estimates of parameters from the likelihood. Assuming a flat prior we can identify the posterior distribution with the likelihood, Eq. (3.7). We expand the $\ln\mathcal{L}$ near the peak with a Taylor series up to the quadratic term:

$$\ln\mathcal{L} = \ln\mathcal{L}(\theta_0) + \frac{1}{2}\sum_{ij}(\theta_i - \theta_{i,0})\left.\frac{\partial^2\ln\mathcal{L}}{\partial\theta_i\partial\theta_j}\right|_{\theta_0}(\theta_j - \theta_{j,0}) + \dots \tag{3.8}$$

where the first derivative term obviously vanish in θ_0 since the peak is a local maximum of $\ln\mathcal{L}$. In this way the likelihood surface is locally approximated to a multi-variate Gaussian. The Hessian matrix is then:

$$\mathcal{H}_{ij} = -\frac{\partial^2 \ln\mathcal{L}}{\partial\theta_i \partial\theta_j}. \tag{3.9}$$

It encloses the information about the covariance of the parameter errors and, if it is non-diagonal, also their correlation. We remind that parameters are said to be correlated, or degenerate, if they produce similar effects on the data. Parameter degeneracy is the ambiguity between two or more parameters about their effects on data.

3.2.2 Fisher information matrix

Assuming a model likelihood $\ln\mathcal{L}(x,\theta)$, where $x = (x_1, x_2, \cdots, x_n)$ is an ensemble of n realizations of an aleatory variable and $\theta = \{\theta_i\} \in \mathbb{R}^k$ is a vector of parameters expected by the model, we call score the vector of the first partial derivatives of $\ln\mathcal{L}(x,\theta)$ with respect to θ_i:

$$s(x,\theta) = \left(\frac{\partial \ln\mathcal{L}(x,\theta)}{\partial\theta_1}, \cdots, \frac{\partial \ln\mathcal{L}(x,\theta)}{\partial\theta_k}\right). \tag{3.10}$$

We have that the expectation value of the score is $\langle s(x,\theta)\rangle = 0$ and the variance of the score $\mathrm{Var}(s(x,\theta)) \equiv \mathcal{F}(\theta)$ is a $k \times k$ matrix called Fisher information, with:

$$\mathcal{F}_{ij}(\theta) = -\left\langle \frac{\partial^2 \ln\mathcal{L}(x,\theta)}{\partial\theta_i \partial\theta_j} \right\rangle. \tag{3.11}$$

From Eq. (3.9) one can see immediately that $\mathcal{F} = \langle\mathcal{H}\rangle$.
Given a dataset, suppose now that we want to estimate the uncertainties of the model parameters from it. We have that θ_0 are the true parameter values and $\theta(x)$ are our estimates, which are functions of the data vector x and therefore are also random variables. We expect $\langle\theta\rangle = \theta_0$, meaning that θ are unbiased and that the standard deviations $\sigma_{\theta_i} \equiv (\langle\theta_i^2\rangle - \langle\theta_i\rangle^2)^{1/2}$ are minimized. In the general case we have:

$$\sigma_{ij}^2 \geq (\mathcal{F}^{-1})_{ij}, \tag{3.12}$$

that is the so-called the Cramér-Rao inequality (that is a particular case of the Schwarz inequality [11]). This inequality is the reason why the Fisher matrix method gives the estimate of the smallest error bars. If the likelihood is Gaussian Eq. (3.12) becomes, indeed, an equality (this situation is sometimes called saturation of the Cramér-Rao bound [11]). Then, when we have estimated all parameters simultaneously from the data, the marginalized error for each paramater is:

$$\sigma_{\theta_i} \geq (\mathcal{F}^{-1})^{1/2}_{ii}, \tag{3.13}$$

where the term on the right is the square root of the element ii of the inverse of the Fisher matrix. So Eq. (3.13) is the error estimation for each parameter. For a parameter vector $\theta = \{\theta_k\} = \{\theta_a, \theta_b\}$, where $\theta_a = \{\theta_1, \cdots, \theta_{i-1}\}$ and $\theta_b = \{\theta_i, \cdots, \theta_k\}$, the marginalized distribution over θ_b is the distribution $P(\theta_a)$ obtained averaging the information about θ_b:

$$P(\theta_1, \cdots, \theta_{i-1}) = \int \mathrm{d}\theta_i \cdots \int \mathrm{d}\theta_k P(\theta_1, \cdots, \theta_{i-1}, \theta_i, \cdots, \theta_k). \tag{3.14}$$

It follows that marginalization propagates uncertainties between degenerate parameters.
Eq. (3.13) assumes that the likelihood around its maximum is Gaussian, a condition in general not so trivial (this is infact not often the case in Cosmology). For forecast analysis like this one, where we approximate likelihoods by Gaussian distributions, such condition is obviously valid.

3.2.3 Forecasts

The Fisher matrix is of crucial importance in predicting the cosmological parameter errors from future experiments, allowing feedbacks for the configuration and the possible optimization of the instruments.
Another important property comes from the fact that the Fisher matrix for independent datasets is the sum of the individual Fisher matrices, because the total likelihood for independent datasets is the product of their single

likelihoods. Therefore we can use the complementarity of independent experiments in order to reduce both the parameter uncertanties and the parameter degeneracies because the operations of adding the experimental data and marginalising do not commute. Furthermore it is extremely profitable from the computational poit of view, making all of these aspect easily achievable in term of time costs. These are the reasons why the Fisher matrix approach is so useful in survey design.

3.2.4 Computation of the Fisher matrix

In the case of a Gaussian likelihood, the computation of the Fisher matrix can be done analitically in a quite simple and elegant way and it can be applied to a wide variety of problems in cosmology.
First of all, we rearrange Eq. (3.6) in order to have:

$$-2\ln\mathcal{L} = n\ln(2\pi) + \ln|\det(\mathcal{C})| + (D-y)\mathcal{C}^{-1}(D-y)^T. \tag{3.15}$$

Then, remember that both the mean vector y and the covariance matrix $\mathcal{C}$ depend on the model parameters θ, defining the data matrix $\mathcal{D} \equiv (D-y)(D-y)^T$, dropping the constant $n\ln(2\pi)$ (if one has interest for the confidence levels of the parameters, then that normalization factor is irrelevant [12]) and using the matrix identity $\ln[\det(\mathcal{C})] = \mathrm{Tr}[\ln(\mathcal{C})]$, one can write:

$$2\ln\mathcal{L} = \mathrm{Tr}(\ln\mathcal{C} + \mathcal{C}^{-1}\mathcal{D}). \tag{3.16}$$

In the standard comma notation for derivatives, where $\mathcal{C}_{,i} \equiv \frac{\partial}{\partial\theta_i}\mathcal{C}$ and using the matrix identities $(\mathcal{C}^{-1})_{,i} = \mathcal{C}^{-1}\mathcal{C}_{,i}\mathcal{C}^{-1}$ and $(\ln\mathcal{C}^{-1})_{,i} = \mathcal{C}^{-1}\mathcal{C}_{,i}$, we have:

$$2\mathcal{L}_{,i} = \mathrm{Tr}[\mathcal{C}^{-1}\mathcal{C}_{,i} - \mathcal{C}^{-1}\mathcal{C}_{,i}\mathcal{C}^{-1}\mathcal{D} + \mathcal{C}^{-1}\mathcal{D}_{,i}]. \tag{3.17}$$

Knowing that if we do the evaluation at y we have $\langle D\rangle = y$ and $\langle DD^T\rangle = \mathcal{C} + yy^T$, which gives $\langle\mathcal{D}\rangle = \mathcal{C}$, $\langle\mathcal{D}_{,i}\rangle = 0$ and $\langle\mathcal{D}_{,ij}\rangle \equiv \mathcal{M}_{ij} = y_{,i}y_{,j}^T + y_{,j}y_{,i}^T$, and deriving again Eq. (3.17) and averaging, we obtain (after some simple algebra), the explicit form of the Fisher information matrix:

$$\mathcal{F}_{ij} = \left\langle -\frac{\partial^2\ln\mathcal{L}}{\partial\theta_i\partial\theta_j}\right\rangle = \frac{1}{2}\mathrm{Tr}\left[\mathcal{C}^{-1}\frac{\partial\mathcal{C}}{\partial\theta_i}\mathcal{C}^{-1}\frac{\partial\mathcal{C}}{\partial\theta_j} + \mathcal{C}^{-1}\mathcal{M}_{ij}\right] \tag{3.18}$$

To conclude, in order to have the predicted errors it is necessary to have a fiducial model y, to know how $y = y(\theta)$ and the related covariance matrix.

3.3 Surveys simulation and data analysis

We have focused our attention on the forecasts about future experiments concerning the observation of CMB anisotropies and LSS formation. The main experiment considered is the Cosmic ORigins Explorer[1] (CORE), a proposal for a Class-M space mission in response to the European Space Agency (ESA) Cosmic Vision call for 2015-2025, for the observation of the CMB. Regarding the LSS, we have taken in consideration Euclid, another Class-M mission, that is part of the same ESA's scientific program [13]. Euclid was chosen in October 2011 and its launch is planned for 2020. Furtermore, we have also studied the parameter uncertainties achieved with the *Planck* satellite[2], the latest mission for the CMB observation.

3.3.1 Mock data generation and examination

We have generated our mock data for the CMB and LSS power spectra with the November 2016 release of CAMB[3] (Code for Anisotropies in the Microwave Background) by Antony Lewis and Anthony Challinor [14]. The software is an Einstein-Boltzmann code to predict CMB anisotropies and LSS formation from a set of cosmological parameters.
The fiducial cosmology assumed, whose parameter values are shown in Tab. 3.1, is the ΛCDM flat-Universe model with three massless neutrinos as in the CORE ECO paper [15] and based on the latest constraints by *Planck* [17]. The calculation of the partial derivatives of the power spectra with respect to the parameters of the model in Eq. (3.18) has been done evaluating their

[1] http://coresat.planck.fr/uploads/Main/CORE-M5-proposal-for-posting-v1.pdf
[2] https://www.cosmos.esa.int/documents/387566/387653/Bluebook-ESA-SCI(2005)1_V2.pdf/d364e30e-f85f-4191-a989-fa6b7527ba55
[3] http://camb.info/readme.html

ω_c	ω_b	H_0 [km/s/Mpc]	τ	n_s	$\ln(10^{10}A_s)$
0.1206	0.02214	66.89	0.0581	0.9625	3.053

Table 3.1: The six cosmological parameters of the standard ΛCDM model. The cold dark matter ω_c and the barion ω_b physical density parameters, the Hubble parameter at present time H_0, the optical depth τ at the time of reionization, the amplitude $\ln(10^{10}A_s)$ of the scalar primordial fluctuations power spectrum and its spectral index n_s.

symmetric difference quotient, a numerical approximation of the symmetric derivative:

$$\frac{f(\theta_i + \Delta_i) - f(\theta_i - \Delta_i)}{2\Delta_i} \simeq \left.\frac{\partial f(\theta)}{\partial \theta_i}\right|_{\theta_0}, \tag{3.19}$$

Here $\theta_0 = \langle\theta_{\rm mod}\rangle$,where $\theta_{\rm mod} = \{\theta_{\Lambda\rm CDM}, \theta_{\rm ext}\}$ are the model parameters, $\theta_{\Lambda\rm CDM} = \{\omega_c, \omega_b, H_0, \tau, n_s, \ln(10^{10}A_s)\}$ are the cosmological parameters of the standard ΛCDM model and $\theta_{\rm ext}$ are the extra parameters studied.
We have checked the numerical stability of the derivatives using different steps $\epsilon = 3 \cdot 10^{-1}, 3 \cdot 10^{-2}, 3 \cdot 10^{-3}$. Furthermore, we have also used another formula for the derivatives, the so-called five-point stencil, a more precise numerical approximation, and checked the different steps for these cases. The comparison of all these combinations has shown that the results obtained with Eq. (3.19) and $\epsilon = 3 \cdot 10^{-2}$ were enough (in some cases the best) for achieving an acceptable level of accuracy. In Appendix A we show the trend of the derivatives of the power spectra derived from CMB and LSS and also some example of different steps and different numerical methods compared.

3.3.2 CMB

The observables considered for the Fisher forecasts on the CMB anisotropies are the temperature and E-mode anisotropies, plus their correlation. Furthermore, both the lensing potential related to the shear affecting the CMB

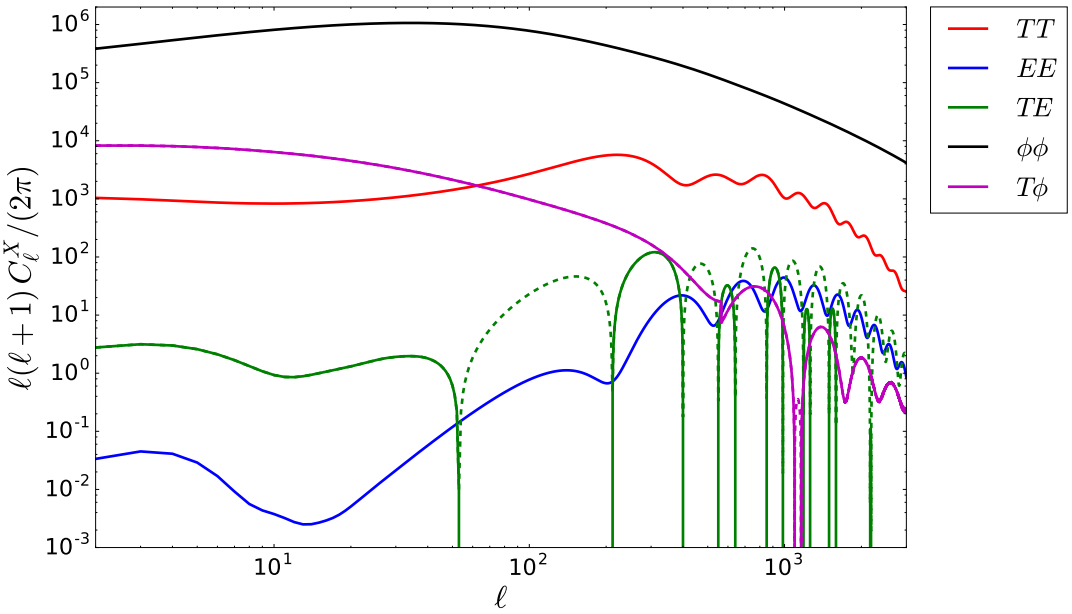

Figure 3.1: Angular power spectra for the CMB anisotropies. Temperature auto-spectrum (red), E-mode polarization auto-spectrum (blue), lensing potential auto-spectrum (black), temperature and E-mode cross-correlation (green), temperature and lensing cross-correlation (magenta). All the spectra are obtained from the fiducial ΛCDM model, whose parameters are those shown in Tab. 3.1.

signal and the lensing correlation with the temperature are taken in consideration. All of these observables are analysed through their angular power spectra, which are shown in Fig. 3.1. We have that the total mock angular power spectra are the sum of signal and noise $\bar{C}_\ell^X = C_\ell^X + N_\ell^X$. The noise is modelled as $N_\ell^X = w_X^{-1} b_\ell^{-2}$, where $b_\ell^2 = \exp[-\ell(\ell+1)\theta_{FWHM}^2/8\ln 2]$ is the Gaussian beam window function, θ_{FWHM} is the Full Width Half Maximum (FWHM) of the beam and w_X is the inverse square of the detector noise level. In the case of multiple frequency channel the total noise is obtained combining the single ones with an inverse noise variance weighting [16]. We assume negligible noise terms for cross-correlated power spectra.

The noise of the lensing potential $N_\ell^{\phi\phi}$ is obtained in the following estima-

tion procedure suggested by Hu & Okamoto [18]. The lensing potential is reconstructed from the observed CMB anisotropies (in our case, the lensed mock data) and the related noise matrix is calculated as:

$$\begin{aligned}\mathcal{N}_{\alpha\beta}(L) =& \frac{A_\alpha(L)A_\beta(L)}{L^2}\int \frac{\mathrm{d}^2\ell_1}{(2\pi)^2}F_\alpha(\ell_1,\ell_2) \\ &\times\left[F_\beta(\ell_1,\ell_2)C_{\ell_1}^{x_\alpha x_\beta}C_{\ell_2}^{x'_\alpha x'_\beta}+F_\beta(\ell_2,\ell_1)C_{\ell_1}^{x_\alpha x'_\beta}C_{\ell_2}^{x'_\alpha x_\beta}\right],\end{aligned} \tag{3.20}$$

with the introduction of a normalization factor:

$$A_\alpha(L) = L^2\left[\int \frac{\mathrm{d}^2\ell_1}{(2\pi)^2}f_\alpha(\ell_1,\ell_2)F_\alpha(\ell_1,\ell_2)\right]^{-1}, \tag{3.21}$$

and with the minimum variance filter $F_\alpha(\ell_1,\ell_2)$ calculated as:

$$F_\alpha(\ell_1,\ell_2) = \frac{C_{\ell_1}^{x'x'}C_{\ell_2}^{xx}f_\alpha(\ell_1,\ell_2) - C_{\ell_1}^{xx'}C_{\ell_2}^{xx'}f_\alpha(\ell_2,\ell_1)}{C_{\ell_1}^{xx}C_{\ell_2}^{x'x'}C_{\ell_1}^{x'x'}C_{\ell_2}^{xx} - \left(C_{\ell_1}^{xx'}C_{\ell_2}^{xx'}\right)^2}. \tag{3.22}$$

Here $x, x' = \{T, E, B\}$, α denotes the xx' pairing, $L = \ell_1 + \ell_2$ and $f_\alpha(\ell_1,\ell_2)$ is a coupling strength factor related to the pair α with respect to the multipole moments ℓ_1 and ℓ_2. The final (minimum variance) noise power spectrum for lensing reconstruction is:

$$N_{\mathrm{mv}}(L) = \frac{1}{\sum_{\alpha\beta}\mathcal{N}^{-1}_{\alpha\beta}}, \tag{3.23}$$

where, in our case, the anisotropy variable pairs are $\{TT, EE, BB, TE, TB, EB\}$. Once the Fisher matrix for the CMB power spectra is calculated, it is useful to rewrite it in the following form:

$$\mathcal{F}_{ij}^{CMB} = \sum_{\ell=2}^{\ell_{max}}\sum_{X,Y}\frac{\partial\mathcal{C}_\ell^X}{\partial\theta_i}\mathscr{C}_\ell^{-1}\frac{\partial\mathcal{C}_\ell^Y}{\partial\theta_j}, \tag{3.24}$$

where X, Y denote the different auto or cross-correlated spectra involved into the analysis and $\mathscr{C}$ is sometimes called the angular power spectrum covariance matrix at the ℓ-th multipole.

We show now the different cases for which we have calculated the explicit form of the $\mathscr{C}$. The covariance matrix of the mock data for the combination

of all the temperature and E-mode polarization angular power spectra $\bar{\mathcal{C}}_\ell^{TT}$, $\bar{\mathcal{C}}_\ell^{TE}$ and $\bar{\mathcal{C}}_\ell^{EE}$ is:

$$\mathcal{C}_\ell = \begin{pmatrix} \bar{C}_\ell^{TT} & \bar{C}_\ell^{TE} \\ \bar{C}_\ell^{TE} & \bar{C}_\ell^{EE} \end{pmatrix} \tag{3.25}$$

and, after the computation of the Eq. (3.24), we obtain:

$$\mathscr{C}_\ell = \frac{2}{(2\ell+1)f_{\rm sky}} \begin{pmatrix} (\bar{C}_\ell^{TT})^2 & (\bar{C}_\ell^{TE})^2 & \bar{C}_\ell^{TT}\bar{C}_\ell^{TE} \\ (\bar{C}_\ell^{TE})^2 & (\bar{C}_\ell^{EE})^2 & \bar{C}_\ell^{TE}\bar{C}_\ell^{EE} \\ \bar{C}_\ell^{TT}\bar{C}_\ell^{TE} & \bar{C}_\ell^{TE}\bar{C}_\ell^{EE} & \frac{1}{2}\left[(\bar{C}_\ell^{TE})^2 + \bar{C}_\ell^{TT}\bar{C}_\ell^{EE}\right] \end{pmatrix}. \tag{3.26}$$

We can notice that Eq. (3.26) is more complicated that what one would have obtained by assuming no correlation between temperature and E-mode. The multiplicative factor takes into account both the sampling variance $2/(2\ell+1)$ and the sky fraction $f_{\rm sky}$.

If one wants to add the contribution of the lensing potential auto-correlation angular power spectrum $\bar{C}_\ell^{\phi\phi}$, the covariance matrix of the mock data is now:

$$\mathcal{C}_\ell = \begin{pmatrix} \bar{C}_\ell^{TT} & \bar{C}_\ell^{TE} & 0 \\ \bar{C}_\ell^{TE} & \bar{C}_\ell^{EE} & 0 \\ 0 & 0 & \bar{C}_\ell^{\phi\phi} \end{pmatrix}, \tag{3.27}$$

where we neglet any cross-correlation. The computation of Eq. (3.24) in this case gives us:

$$\mathscr{C}_\ell = \frac{2}{(2\ell+1)f_{\rm sky}} \begin{pmatrix} (\bar{C}_\ell^{TT})^2 & (\bar{C}_\ell^{TE})^2 & \bar{C}_\ell^{TT}\bar{C}_\ell^{TE} & 0 \\ (\bar{C}_\ell^{TE})^2 & (\bar{C}_\ell^{EE})^2 & \bar{C}_\ell^{TE}\bar{C}_\ell^{EE} & 0 \\ \bar{C}_\ell^{TT}\bar{C}_\ell^{TE} & \bar{C}_\ell^{TE}\bar{C}_\ell^{EE} & \frac{1}{2}\left[(\bar{C}_\ell^{TE})^2 + \bar{C}_\ell^{TT}\bar{C}_\ell^{EE}\right] & 0 \\ 0 & 0 & 0 & (\bar{C}_\ell^{\phi\phi})^2 \end{pmatrix}. \tag{3.28}$$

In this second result is evident how the absence of cross-correlation obviously leads no complications in the adjustment of the final matrix.

The case with both E-mode and B-mode polarizations would be analogous to the previous one (just replacing the term $\bar{C}_\ell^{\phi\phi}$ with $\bar{C}_\ell^{BB}$) because, for parity

conserving cosmologies, both the terms C_ℓ^{TB} and C_ℓ^{EB} are exactly equal to zero.

For a combination of both the lensing auto-correlation and the temperature-lensing cross-correlation, we have:

$$\mathcal{C}_\ell = \begin{pmatrix} \bar{C}_\ell^{TT} & \bar{C}_\ell^{TE} & \bar{C}_\ell^{T\phi} \\ \bar{C}_\ell^{TE} & \bar{C}_\ell^{EE} & 0 \\ \bar{C}_\ell^{T\phi} & 0 & \bar{C}_\ell^{\phi\phi}, \end{pmatrix}, \tag{3.29}$$

and consequently:

$$\mathscr{C}_\ell = \frac{2}{(2\ell+1)f_{\rm sky}} \begin{pmatrix} \Xi_{TT,TT} & \Xi_{TT,EE} & \Xi_{TT,TE} & \Xi_{TT,T\phi} & \Xi_{TT,\phi\phi} \\ \Xi_{TT,EE} & \Xi_{EE,EE} & \Xi_{TE,EE} & 0 & 0 \\ \Xi_{TT,TE} & \Xi_{TE,EE} & \Xi_{TE,TE} & 0 & 0 \\ \Xi_{TT,T\phi} & 0 & 0 & \Xi_{T\phi,T\phi} & \Xi_{T\phi,\phi\phi} \\ \Xi_{TT,\phi\phi} & 0 & 0 & \Xi_{T\phi,\phi\phi} & \Xi_{\phi\phi,\phi\phi} \end{pmatrix}, \tag{3.30}$$

where the autocorrelation coefficients are given by:

$$\begin{aligned} \Xi_{TT,TT} &= (\bar{C}_\ell^{TT})^2 - \frac{2(\bar{C}_\ell^{TE})^2(\bar{C}_\ell^{TP})^2}{\bar{C}_\ell^{EE}\bar{C}_\ell^{\phi\phi}}, \\ \Xi_{EE,EE} &= (\bar{C}_\ell^{EE})^2, \\ \Xi_{TE,TE} &= \frac{1}{2}[(\bar{C}_\ell^{TE})^2 + \bar{C}_\ell^{TT}\bar{C}_\ell^{EE}] - \frac{\bar{C}_\ell^{EE}(\bar{C}_\ell^{T\phi})^2}{2\bar{C}_\ell^{\phi\phi}}, \\ \Xi_{T\phi,T\phi} &= \frac{1}{2}[(\bar{C}_\ell^{T\phi})^2 + \bar{C}_\ell^{TT}\bar{C}_\ell^{\phi\phi}] - \frac{\bar{C}_\ell^{\phi\phi}(\bar{C}_\ell^{TE})^2}{2\bar{C}_\ell^{EE}}, \\ \Xi_{\phi\phi,\phi\phi} &= (\bar{C}_\ell^{\phi\phi})^2, \end{aligned} \tag{3.31}$$

and the cross-correlated ones are

$$\begin{aligned}
\Xi_{TT,EE} &= (\bar{C}_\ell^{TE})^2, \\
\Xi_{TT,TE} &= \bar{C}_\ell^{TE}\left[\bar{C}_\ell^{TT} - \frac{(\bar{C}_\ell^{T\phi})^2}{\bar{C}_\ell^{\phi\phi}}\right], \\
\Xi_{TE,EE} &= \bar{C}_\ell^{TE}\bar{C}_\ell^{EE}, \\
\Xi_{TT,\phi\phi} &= (\bar{C}_\ell^{T\phi})^2, \\
\Xi_{TT,T\phi} &= \bar{C}_\ell^{T\phi}\left[\bar{C}_\ell^{TT} - \frac{(\bar{C}_\ell^{TE})^2}{\bar{C}_\ell^{EE}}\right], \\
\Xi_{T\phi,\phi\phi} &= \bar{C}_\ell^{T\phi}\bar{C}_\ell^{\phi\phi}.
\end{aligned} \tag{3.32}$$

We have not considered the full case of a $\mathcal{C}_\ell$ with the E-mode polarization and lensing cross-correlation term $C_\ell^{E\phi}$ because it is beyond the observational capabilities of the nearly future experiments and its effect would improve our constraints less than 1%.

3.3.3 Spectroscopic galaxy surveys

We consider as observables in our forecasts for the LSS nine indipendent galaxy clustering power spectra, shown in Fig. 3.2, from a range of nine redshift bins.

In this analysis we follow the same methodology in Ballardini et al. [21]. The simplest model for the observed galaxy power spectrum assumes a scale-independent and linear galaxy bias, with redshift space distorsions not associated to the Hubble flow but due to small peculiar velocities:

$$\mathcal{P}_g(k,\mu,z) = b(z)^2[1+\beta(k,z)\mu^2]^2\mathcal{P}_m(k,z)\exp(-k^2\mu^2\sigma_{\rm tot}^2) \tag{3.33}$$

where b is the galaxy bias, which relates the dark matter density field to the galaxy number density one, $\beta \equiv f/b$, with $f \equiv {\rm dln}G(z)/{\rm dln}a$ is the growth rate and $G(z)$ is the growth factor, μ denotes the cosine of the angle between the line of sight and the wave vector and $\mathcal{P}_m(k,z)$ represents the dark matter power spectrum. We also define $\sigma_{\rm tot} = \sqrt{\sigma_v^2 + \sigma_r^2}$, where $\sigma_r \simeq \sigma(z)c/H(z)$ is the spectrometric redshift error and σ_v is the redshit error due to galaxy

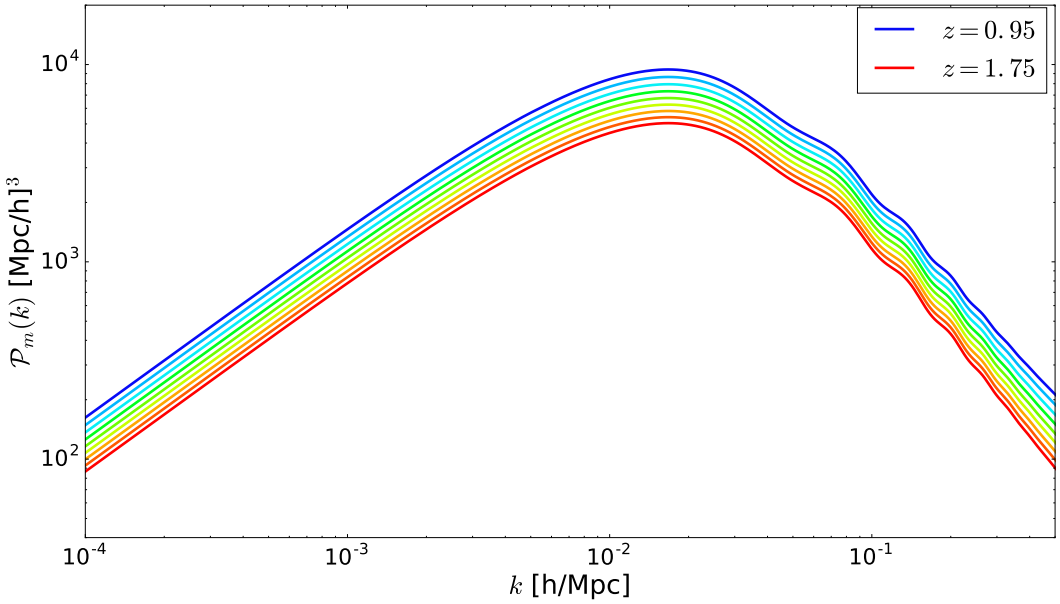

Figure 3.2: Power spectra of the dark matter density field $\mathcal{P}_m$ for the nine redshift bins and for the fiducial ΛCDM model. At higher k it is possible to see both the shape of the BAO and the deviation from the self-similarity growth of the power spectra for the beginning of the non-linar regime, both due to the physics implemented in CAMB code.

velocity dispersion. The former is parametrized as $\sigma(z) = \bar{\sigma}_z(1+z)$ where $\bar{\sigma}_z$ is the average redshift error within a redishift bin, while for the latter it has been chosen a value of $\sigma_v = 7\,\mathrm{Mpc}$, corresponding to a velocity dispersion of $\sim 500\,\mathrm{km/s}$. For a Poisson sampled density field, a constant shot-noise contribution to the power $N_{\mathrm{shot}}(z)$, due to the finite number of galaxies per bin, must be added:

$$\mathcal{P}_{\mathrm{obs}}(k,\mu,z) = \mathcal{P}_g(k,\mu,z) + N_{\mathrm{shot}}(z). \tag{3.34}$$

In order to include the effects due to the incorrect assumption of the reference cosmology with respect to the fiducial one, Eq. (3.34) becomes:

$$\widetilde{\mathcal{P}}_{\mathrm{obs}}(k^{\mathrm{ref}},\mu^{\mathrm{ref}},z) = \left(\frac{D_A^{\mathrm{ref}}(z)}{D_A(z)}\right)^2 \frac{H(z)}{H^{\mathrm{ref}}(z)}\mathcal{P}_g(k,\mu,z) + N_{\mathrm{shot}}(z), \tag{3.35}$$

where the prefactor is the Alcock-Paczynski effect [22] and where the wavenumbers k and the direction cosine μ are related by their reference cosmology counterparts by:

$$k = k^{\mathrm{ref}}\sqrt{\left(\frac{H(z)}{H^{\mathrm{ref}}(z)}\mu^{\mathrm{ref}}\right)^2 - \left(\frac{D_A^{\mathrm{ref}}(z)}{D_A(z)}\right)^2 [(\mu^{\mathrm{ref}})^2 - 1]}, \tag{3.36}$$

and:

$$\mu = \mu^{\mathrm{ref}}\left(\frac{H(z)}{H(z)^{\mathrm{ref}}}\right)^2 \frac{k^{\mathrm{ref}}}{k}. \tag{3.37}$$

We report some of the parameters related to the observed power spectra in Fig. 3.3. We assume that the density field has a Gaussian statistics and uncorrelated Fourier modes, therefore the Fisher matrix for the broadband power spectrum, for a given redshift bin with $\bar{z}$ as central value, is:

$$\begin{aligned}\mathcal{F}_{ij}^{gg}(\bar{z}) &= \int_{k_{min}}^{k_{max}} \frac{\mathrm{d}^3k}{2(2\pi)^3} \left.\frac{\partial \ln\widetilde{\mathcal{P}}_{\mathrm{obs}}(k,\mu,\bar{z})}{\partial\theta_i}\right|_{\theta_0} \left.\frac{\partial \ln\widetilde{\mathcal{P}}_{\mathrm{obs}}(k,\mu,\bar{z})}{\partial\theta_j}\right|_{\theta_0} V_{\mathrm{eff}}(k,\mu,\bar{z}) \\ &= \int_{k_{min}}^{k_{max}} \frac{k^2\mathrm{d}k}{(2\pi)^2} \int_0^1 \mathrm{d}\mu \left.\frac{\partial \ln\widetilde{\mathcal{P}}_{\mathrm{obs}}(k,\mu,\bar{z})}{\partial\theta_i}\right|_{\theta_0} \left.\frac{\partial \ln\widetilde{\mathcal{P}}_{\mathrm{obs}}(k,\mu,\bar{z})}{\partial\theta_j}\right|_{\theta_0} V_{\mathrm{eff}}(k,\mu,\bar{z}),\end{aligned} \tag{3.38}$$

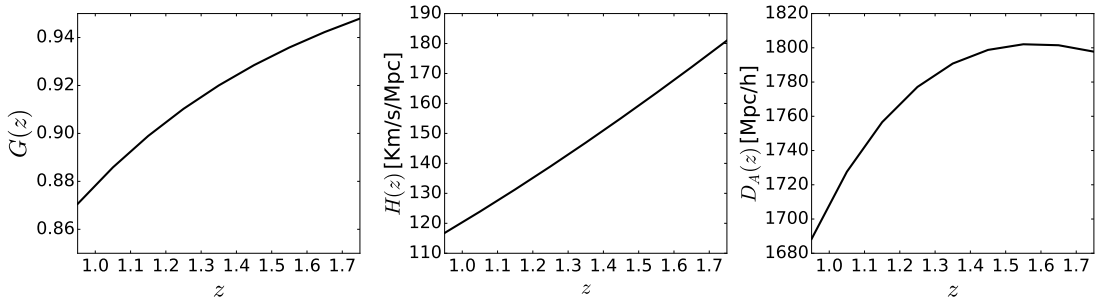

Figure 3.3: The growth factor $G(z)$, the Hubble parameter $H(z)$ and the angular distance $D_A(z)$ for the fiducial ΛCDM model in the redshift range considered.

where the effective volume of the survey $V_{\rm eff}$ in Fourier space, which determines the mode counts, is:

$$\begin{aligned} V_{\rm eff}(k,\mu,\bar{z}) &= \int \frac{\mathrm{d}^3 r}{(2\pi)^3} \left[\frac{\bar{n}_g(\bar{z})\widetilde{\mathcal{P}}_{obs}(k,\mu,\bar{z})}{\bar{n}_g(\bar{z})\widetilde{\mathcal{P}}_{obs}(k,\mu,\bar{z})+1} \right]^2 \\ &\simeq \left[\frac{\bar{n}_g(\bar{z})\widetilde{\mathcal{P}}_{obs}(k,\mu,\bar{z})}{\bar{n}_g(\bar{z})\widetilde{\mathcal{P}}_{obs}(k,\mu,\bar{z})+1} \right]^2 V_{\rm surv}(\bar{z}), \end{aligned} \tag{3.39}$$

where $\bar{n}_g$ is the average number density of tracers in a specific redshift bin and $V_{\rm surv}$ is the geometrical volume of the survey, that can be written as:

$$V_{\rm surv} = \frac{4\pi}{3} f_{\rm sky}(\chi^3(z_i) - \chi^3(z_{i+1})) \tag{3.40}$$

where $\chi(z_i)$ is the comoving distance. We consider the information up to the quasi non-linear scales, i.e. $k_{\rm max} = 0.2$ h/Mpc in all redshift bins, while $k_{\rm min}(\bar{z}_i) = 2\pi/\sqrt[3]{V_{\rm surv}(\bar{z}_i)}$, set in each redshift bin by the corresponding slice volume (intuitively, one cannot obtain information about scales larger than the volume observed). Furthermore, in order to neglect the possible correlation between near wavenumbers, we consider a linear binning scheme for the wave-number, adopting the minimum $\Delta k = 1.4/\sqrt[3]{V_{\rm surv}(\bar{z}_i)}$ in accord to [23]. Therefore we can rewrite the (3.38) as a binned sum over k and μ:

$$\mathcal{F}^{gg}_{ij}(\bar{z}) = \sum_{k,\mu} \left. \frac{\partial \ln \widetilde{\mathcal{P}}_{\rm obs}(k,\mu,\bar{z})}{\partial \theta_i} \right|_{\theta_0} \mathscr{C}_k^{-1}(\bar{z}) \left. \frac{\partial \ln \widetilde{\mathcal{P}}_{\rm obs}(k,\mu,\bar{z})}{\partial \theta_j} \right|_{\theta_0}, \tag{3.41}$$

where:

$$\mathscr{C}_k(\bar{z}) = \frac{(2\pi)^2}{k^2 \Delta k \Delta\mu} V_{\rm eff}^{-1}(k,\mu,\bar{z}). \tag{3.42}$$

As one can see, the matrix $\mathscr{C}_k(\bar{z})$ is reduced to a scalar, because there are no cross-correlation terms between the power spectra of each redshift bin. The derivative term in (3.41) is:

$$\begin{aligned}\frac{\partial \ln\widetilde{\mathcal{P}}_{\rm obs}(k,\mu,\bar{z})}{\partial\theta_i} \simeq \frac{\partial \ln\mathcal{P}_m(k,\bar{z})}{\partial\theta_i} + \frac{2\mu^2}{b(\bar{z})[1+\beta(k,\bar{z})2\mu^2]}\frac{\partial f(k,\bar{z})}{\partial\theta_i} \\ + \left[1 + \frac{4\beta(k,\bar{z})\mu^2}{1+\beta(k,\bar{z})\mu^2}(1-\mu^2) + \mu^2\frac{\partial \ln\mathcal{P}_m(k,\bar{z})}{\partial \ln k}\right]\frac{\partial \ln H(\bar{z})}{\partial\theta_i} \\ - \left[2 - \frac{4\beta(k,\bar{z})\mu^2}{1+\beta(k,\bar{z})\mu^2}(1-\mu^2) + (1-\mu^2)\frac{\partial \ln\mathcal{P}_m(k,\bar{z})}{\partial \ln k}\right]\frac{\ln D_A(\bar{z})}{\partial\theta_i} \\ + \frac{2}{1+\beta(k,\bar{z})\mu^2}\frac{\partial \ln b(\bar{z})}{\partial\theta_i} + \frac{1}{\widetilde{\mathcal{P}}_{\rm obs}(k,\mu,\bar{z})}\frac{\partial N_{\rm shot}(\bar{z})}{\partial\theta_i} - k^2\mu^2\frac{\partial\sigma^2_{\rm tot}}{\partial\theta_i},\end{aligned} \tag{3.43}$$

The total array of independent parameters $\theta = \{\theta_i\}$ for which we calculate the total Fisher matrix can be divided in two subgroups $\{\theta_i\} = \{\theta_{\rm mod}, \theta_{\rm nui}\}$, where $\theta_{\rm nui} = \{b, N_{\rm shot}, \sigma^2_{\rm tot}\}$ are the nuisance parameters, taken per redshift bin in order to avoid any prior information on them. The total Fisher matrix is then:

$$\mathcal{F}^{gg}_{\rm tot} = \begin{pmatrix} A_{\theta_{\rm mod},\theta_{\rm mod}} & B_{\theta_{\rm mod},b} & B_{\theta_{\rm mod},N_{\rm shot}} & B_{\theta_{\rm mod},\sigma^2_{\rm tot}} \\ B^T_{\theta_{\rm mod},b} & C_{b,b} & C_{b,N_{\rm shot}} & C_{b,\sigma^2_{\rm tot}} \\ B^T_{\theta_{\rm mod},N_{\rm shot}} & C_{b,N_{\rm shot}} & C_{N_{\rm shot},N_{\rm shot}} & C_{N_{\rm shot},\sigma^2_{\rm tot}} \\ B^T_{\theta_{\rm mod},\sigma^2_{\rm tot}} & C_{b,\sigma^2_{\rm tot}} & C_{N_{\rm shot},\sigma^2_{\rm tot}} & C_{\sigma^2_{\rm tot},\sigma^2_{\rm tot}} \end{pmatrix} \tag{3.44}$$

where $A_{\theta_{\rm mod},\theta_{\rm mod}}$ is a $n \times n$ matrix, where $n = \dim(\theta_{\rm mod})$, with the auto- and cross-correlation terms related to the model parameters, $B_{\theta_{\rm mod},\theta_{\rm nui}}$ are $n \times 9$ matrices with the cross-correlation terms between model and nuisance at each redshift and $C_{\theta_{\rm nui},\theta_{\rm nui}}$ are 9×9 diagonal matrix with the auto- and cross-correlation terms for each nuisance parameter at each redshift. In this analysis we assume that nuisance parameters do not depend on $\theta_{\rm mod}$ and so we marginalize the Fisher matrix over $\theta_{\rm nui}$.

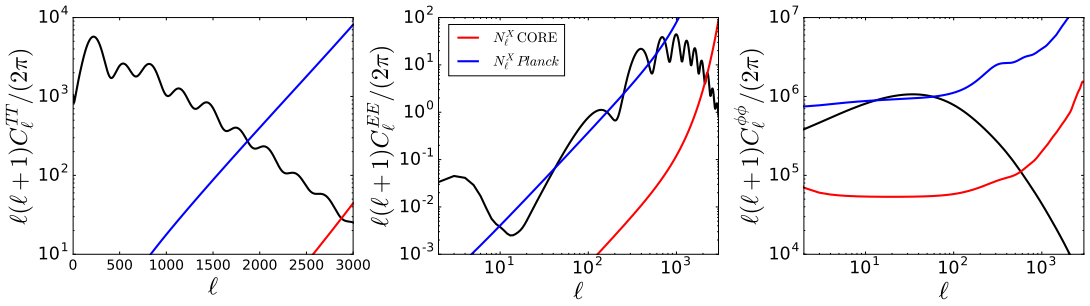

Figure 3.4: Noise of the auto-correlation angular power spectra for CORE (red) and *Planck* (blue). The improvement in the scientific instrument will make possible to detect most of the E-mode polarization and to achieve an impressive improvement in the recostruction of the lensing potential.

3.3.4 Experimental configuration

We report the specifications for each survey we have simulated. The simulated power spectra of the CMB are obtained for CORE in a multipole range of $\ell_{\rm max}^{\rm CORE} = 3000$ and with a sky fraction $f_{\rm sky}^{\rm CORE} = 0.7$, together with the values on Tab. 3.2 to the proposed angular resolution and sensibility.
In the same table we show also the *Planck* specifications, for which the multipole range is $\ell_{\rm max}^{\rm Planck} = 2500$ and with a sky fraction $f_{\rm sky}^{\rm Planck} = 0.75$ (taken from *Planck* bluebook). We have chosen for CORE one third of its total frequency channels, opting for central ones, wich have an higher signal-to-noise ratio. In this way we assume that the channels on sides are used to clean the foregrounds. We have adopted the same approach for *Planck*, choosing only one of the eight channels. In Fig. 3.4 we compare the reduction of the noise contributions expected for CORE with respect to *Planck*.

The observed galaxy clustering power spectra are simulated in a redshift range from $z_{\rm min} = 0.9$ to $z_{\rm max} = 1.8$ with nine equally spaced bins, while in μ we considered 10 bins $\Delta\mu$ between 0 and 1. The sky fraction is $f_{\rm sky} = 15000/(4\pi)\,{\rm deg}^2{\rm rad}^{-2} \simeq 0.36$. The number of galaxies per redshift bin and their bias in Table 3.2 are taken from Pozzetti et al. [24] considering a luminosity selection function compatible with the one expected for Euclid. In

our analysis we use a number of galaxies per redshift bin $\Delta N_g(\bar{z}_i) f_{\rm eff}$, where $f_{\rm eff} = 0.7$ is a completeness factor which takes into account the possible incomplete observation of all the galaxies.

CORE	Channel [GHz]	$\theta_{\rm FWHM}$ [arcmin]	w_T [μK arcmin]	w_E [μK arcmin]	Euclid $\bar{z}_i$	$\Delta N_g(\bar{z}_i)$	$b(\bar{z}_i)$
	130	8.51	3.9	5.5	0.95	7353	1.318
	145	7.68	3.6	5.1	1.05	6552	1.376
	160	7.01	3.7	5.2	1.15	5794	1.434
		6.95	3.6	5.1	1.25	5097	1.493
	195	5.84	3.5	4.9	1.35	4281	1.552
	220	5.23	3.8	5.4	1.45	3447	1.612
Planck	Channel	$\theta_{\rm FWHM}$	w_T	w_E	1.55	2782	1.673
	[GHz]	[arcmin]	[μK arcmin]	[μK arcmin]	1.65	2253	1.733
	143	7.3	33.0	70.2	1.75	1831	1.794

Table 3.2: On the left side, FWHM of the Gaussian beam window function $\theta_{\rm FWHM}$ and inverse square of the detector noise level w_T, w_E on a steradian patch of the T- and E-maps for the frequency coverage expected for CORE. Same specifications for *Planck*. On the right, regarding Euclid, the simulated number of galaxies observed $\Delta N_g(\bar{z}_i)$ and their bias factor $b(\bar{z}_i)$ for each redshift bin, centered in $\bar{z}_i$.

Chapter 4

Contraints on cosmological parameters with CORE and Euclid

In this chapter we present the uncertainties in the cosmological parameters predicted for CORE with the Fisher approach described in Chapter 3. We use the simulated measurements of CMB temperature, E-mode polarization anisotropies angular power spectra together with their cross-correlation. Moreover, we consider the information from the CMB lensing power spectrum. We also discuss the results of the joint forecasts for CORE in combination with the clustering power spectrum expected from Euclid. In order to compare the capabilities of the CORE+Euclid combination with *Planck*+Euclid, we have simulated also the latter data combination.
Furthermore, in order to test the robustness of our results based on the Fisher approach where possible, we made a comparison with public results which were obtained with a Markov Chain Monte Carlo (MCMC) approach to cosmological parameter estimation [33, 36]. This comparison between the Fisher and the MCMC approaches at the sensitivities of future experiments is also a critical result.

4.1 ΛCDM model

We report below the most recent contraints on the cosmological parameters of the ΛCDM model from Planck Collaboration [17].
The physical density parameters of baryons and CDM are respectively:

$$\omega_b = 0.002214 \pm 0.00022 \qquad (68\%\ \text{CL, } \textit{Planck}\ \text{TT+SIMlow}). \tag{4.1}$$

and:

$$\omega_c = 0.1207 \pm 0.0021 \qquad (68\%\ \text{CL, } \textit{Planck}\ \text{TT+SIMlow}), \tag{4.2}$$

the Hubble parameter at present time:

$$H_0 = 66.88 \pm 0.91\ [\text{km/s/Mpc}] \quad (68\%\ \text{CL, } \textit{Planck}\ \text{TT+SIMlow}), \tag{4.3}$$

the reionization optical depth:

$$\tau = 0.0581 \pm 0.0094 \qquad (68\%\ \text{CL, } \textit{Planck}\ \text{TT+SIMlow}). \tag{4.4}$$

The spectral index and the amplitude of the scalar power spectrum measured at the pivot scale $k_* = 0.05\,\text{Mpc}^{-1}$ are respectively:

$$n_s = 0.9624 \pm 0.0057 \qquad (68\%\ \text{CL, } \textit{Planck}\ \text{TT+SIMlow}), \tag{4.5}$$

and:

$$\ln(10^{10} A_s) = 3.053 \pm 0.019 \quad (68\%\ \text{CL, } \textit{Planck}\ \text{TT+SIMlow}). \tag{4.6}$$

4.1.1 Contraints for ΛCDM model

We start by showing the results of the Fisher approach for the standard ΛCDM cosmological model. In Tab. 4.1 we show the 68% CL constraints for the six standard parameters of the LCDM models for CORE. In addition, we report the constraints obtained from a full MCMC forecats from Tab.4

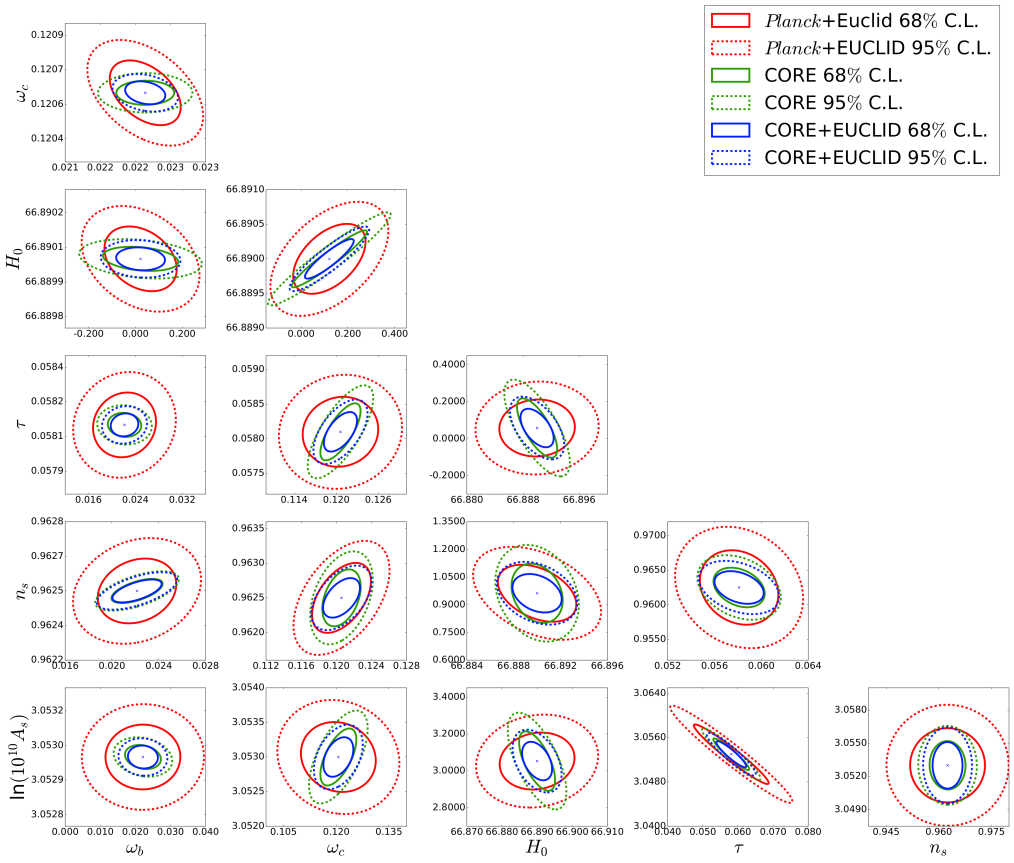

Figure 4.1: Forecast 68% (solid line) and 95% (dashed line) CL 2D marginalized contours of the ΛCDM cosmological parameters for CORE (green), CORE+Euclid (blue) and *Planck*+Euclid (red).

of [36], labelled as CORE-M5. In Fig. 4.1 we show the 2D marginalized contours of the cosmological parameters, i.e. the contours of the 2D gaussian distribution averaged over all but two parameters. The reduction of the area inside the contours are indicative of a better parameter constraining and the variation of the angle of the ellispes implies that the configurations show different degeneracies between parameters.

The errors obtained at 68% CL for the six parameters of ΛCDM model are $\sim 2-5$ times smaller than those reported above for *Planck* and they are

in agreement with the MCMC forecasts for CORE-M5 experimental configuration. We have therefore verified that the Fisher information methodology can be used in place of MCMC methods to contrain parameters cosmology in vanilla ΛCDM model, being more practical and cheaper in terms of computational time.

From Tab. 4.1, we see that CORE would perform better even than the combination *Planck*+Euclid, whose uncertainties are $\sim 1.2 - 2.7$ greater than ones obtained with CORE alone. The exception are ω_c and H_0, for which the LSS information introduced by Euclid can break their degeneracies much better than CMB data alone. Moreover, the precision achieved with the combination of CORE+Euclid information help to further reduce of about $10 - 30\%$ the errors.

The major contribution in breaking parameter degeneracy comes for the hubble parameter, the DM physical density and the amplitude of the scalar primordial fluctuation, thanks to the information about the matter content given by the CMB lensing and galaxy clustering. Moreover, because of the strong degeneracy between A_s and τ in the CMB physics, we can see a reduction in the uncertaintes due to better contraints on A_s from the matter power spectrum information (also if it does not depend on τ). For what concerns the scalar spectral index, the combination of CMB and LSS observation from these two surveys slightly reduces its error.

4.2 Spatial curvature

The standard ΛCDM cosmology assumes a RW metric with a flat 3-dimensional space. We now want to test this geometry assumption. We therefore investigate the constraints on the spatial curvature density parameter Ω_K from future cosmological surveys, defined for ΛCDM models as:

$$\Omega_K \equiv 1 - \Omega_m - \Omega_\Lambda = -\frac{K}{a^2 H^2}, \tag{4.7}$$

The previous definition implies that an open Universe has $\Omega_K > 0$ and a closed one has $\Omega_K < 0$. The parameter Ω_K decreases exponentially with

ΛCDM							
	CORE		CORE-M5 (MCMC)	CORE+Euclid		*Planck*+Euclid	
	T,E	T,E,ϕ	T,E+$\phi\phi$	T,E+$\mathcal{P}(k)$	T,E,ϕ+$\mathcal{P}(k)$	T,E+$\mathcal{P}(k)$	T,E,ϕ+$\mathcal{P}(k)$
$10^6\,\sigma(\omega_b)$	37 [0.017]	34 [0.015]	37 [0.0017]	33 (0.89)	33 (0.97)	93 (2.51)	92 (2.71)
$10^5\,\sigma(\omega_c)$	65 [0.0054]	27 [0.0022]	27 [0.0022]	25 (0.38)	19 (0.70)	34 (0.52)	33 (1.22)
$10^2\,\sigma(H_0)$	25 [0.0037]	11 [0.0016]	11 [0.0016]	9.0 (0.36)	6.9 (0.63)	10 (0.40)	10 (0.91)
$10^4\,\sigma(\tau)$	20 [0.034]	19 [0.033]	20 [0.034]	19 (0.95)	16 (0.84)	38 (1.90)	35 (1.84)
$10^4\,\sigma(n_s)$	18 [0.0019]	14 [0.0015]	14 [0.0015]	15 (0.83)	14 (1.00)	22 (1.22)	22 (1.57)
$10^4\,\sigma\left(\ln(10^{10}A_s)\right)$	42 [0.0014]	34 [0.0011]	35 [0.0011]	40 (0.95)	28 (0.82)	75 (1.79)	70 (2.06)
[*]: relative error (*): ratio with respect to CORE $\sigma(\theta_i)$							
$[H_0]$=[km/s/Mpc] T,E: TT+EE+TE ; T,E,P: TT+EE+TE+$\phi\phi$+Tϕ ; $\mathcal{P}$: $\widetilde{\mathcal{P}}_{\rm obs}$							

Table 4.1: Parameter errors (68% CL) for the ΛCDM cosmology from CORE, CORE+Euclid and *Planck*+Euclid. T,E rows show results for the combination of TT,TE and EE spectra. T,E,ϕ rows include the contribution of $\phi\phi$ and $T\phi$ spectra. LSS refers to the inclusion of galaxy clustering power spectra. In brackets we show the ratio between joint errors and CORE counterparts.

time during the inflationary period, while it grows only as a power law during the radiation and matter dominated phases. For this reason the standard prediction is that spatial curvature should be very close to zero today. Some inflationary models predict tiny deviations from zero and the detection of such deviations would have strong consequences for these classes of models. Slow-roll eternal inflation, for istance, predicts a strong bound on the curvature parameter, $|\Omega_K| < 10^{-4}$ [34, 35].
The current value for the spatial curvature parameter is [17]:

$$\Omega_K = -0.053^{+0.044}_{-0.046} \qquad (95\%\ \text{CL, } \textit{Planck}\ \text{TT+SIMlow}), \tag{4.8}$$

always referring to the article of the Planck Collaboration.

4.2.1 Contraints for the curvature parameter

Our results refer to a model in wich the fiducial value of the curvature parameter is $\Omega_K = 0$. The errors of the physical DM density and the Hubble parameters are lower with respect to the values for CORE-M5, while the

other parameters of the vanilla ΛCDM are quite in agreement. We report them in Tab.10 of [36]. Comparing the error related to the spatial curvature with the result from MCMC forecast of CORE-M5, it is suspiciously too much lower. A similar analysis to the one that we have used is described in [39] (the only difference is that all the proposed CORE frequency channels are used) and the resulting uncertainty for Ω_k is ~ 0.0017, in agreement with the CORE-M5 result and more than six times our constraint, shown in Tab.4.2. Leonard et al. [41] show that, using a combination of different future surveys with a Fisher approach it is possible to reach results equal and lower of $\sim 3 \cdot 10^{-4}$, but this can not explain our result. Moreover, we see that there is no difference between the absence or the contribution of lensing potential in CORE constraints, while we know that lensing information should break some degeneracy in parameters related with DM density distribution, including the spatial curvature density parameter. Infact, both ω_K and H_0 uncertainties drop for the lensing contribution.
We have repeated the simulation using a fiducial value $\Omega_K = -0.055$, compatible with the *Planck* estimate for the spatial curvature in Eq. (4.8). The new results, shown in Tab.4.2, are in perfect agreement with CORE-M5 constraints, included the error of the spatial curvature. The degeneracy between ω_K, H_0 and Ω_k is increased and it is possible to see the contribution of lensing information in reducing such degeneracy.

4.3 Spectral index scale dependences

In section (inflazione) we have introduced the primordial power spectrum of scalar perturbation $\mathcal{P}_\mathcal{R}(k)$ as:

$$\mathcal{P}_\mathcal{R}(k) = \frac{k^3}{2\pi^2}|\mathcal{R}_k|^2 = A_s \left(\frac{k}{k_*}\right)^{n_s - 1} . \tag{4.9}$$

ΛCDM+Ω_K					
	CORE ($\Omega_K = 0$)		CORE ($\Omega_K = -0.055$)		CORE-M5 (MCMC)
	T,E	T,E,ϕ	T,E	T,E,ϕ	T,E+$\phi\phi$
$10^6\,\sigma(\omega_b)$	37 [0.017]	35 [0.016]	36 [0.016]	35 [0.016]	40 [0.018]
$10^5\,\sigma(\omega_c)$	65 [0.0054]	28 [0.0023]	69 [0.0057]	57 [0.0047]	67 [0.0056]
$10^2\,\sigma(H_0)$	26 [0.0039]	12 [0.0018]	93 [0.014]	53 [0.0079]	65 [0.010]
$10^4\,\sigma(\tau)$	20 [0.034]	19 [0.033]	21 [0.036]	21 [0.036]	20 [0.034]
$10^4\,\sigma(n_s)$	18 [0.0019]	15 [0.0016]	20 [0.0021]	17 [0.0018]	18 [0.0019]
$10^4\,\sigma\left(\ln(10^{10}A_s)\right)$	42 [0.0014]	34 [0.0011]	45 [0.0015]	43 [0.0014]	43 [0.0014]
$10^4\,\sigma\,(\Omega_k)$	2.6 [-]	2.6 [-]	30 [0.055]	19 [0.035]	19 [-]
	[*]: relative error				
$[H_0]$=[km/s/Mpc]	T,E: TT+EE+TE ;		T,E,P: TT+EE+TE+$\phi\phi$+Tϕ		

Table 4.2: Parameter errors (68% CL) for the extended model ΛCDM+Ω_K. We report the MCMC forecasts for CORE-M5 experimental configuration, from Tab.10.

Using a Taylor expansion around k_* one can rewrite Eq. (4.9) as:

$$\mathcal{P}_{\mathcal{R}}(k) = A_s \left(\frac{k}{k_*}\right)^{n_s - 1 + \frac{1}{2}\frac{\mathrm{d}n_s}{\mathrm{d}\ln k}\ln\left(\frac{k}{k_*}\right) + \frac{1}{6}\frac{\mathrm{d}^2 n_s}{\mathrm{d}\ln k^2}\ln^2\left(\frac{k}{k_*}\right) + \ldots}, \tag{4.10}$$

where $\mathrm{d}n_s/\mathrm{d}\ln k$ and $\mathrm{d}^2 n_s/\mathrm{d}\ln k^2$ are respectively the running of the scalar spectral index and the running of the running of the scalar spectral index, in order to study the possible n_s scale dependence and its influence on $\mathcal{P}_{\mathcal{R}}(k)$. All of these parameters, A_s, n_s and its runnings, are related to the inflationary physics with the slow-roll parameters introduced in section 1.4.3 and therefore they can be written as:

$$\begin{aligned} A_s &= \frac{H^2}{8\,\pi^2 M_{\mathrm{Pl}}^2\,\epsilon\,c_s}, \\ n_s - 1 &= 2\,\eta - 6\,\epsilon, \\ \frac{\mathrm{d}n_s}{\mathrm{d}\ln k} &= -2\,\xi^2 + 16\,\eta\,\epsilon - 24\,\epsilon^2, \\ \frac{\mathrm{d}^2 n_s}{\mathrm{d}\ln k^2} &= 2\,\sigma^3 + 2\,\xi^2(\eta - 12\,\epsilon) - 32\,\epsilon(\eta^2 - 6\,\eta\,\epsilon + 6\,\epsilon^2), \end{aligned} \tag{4.11}$$

where we have introduced:

$$\begin{aligned}\xi^2 &\equiv M_{\rm Pl}^4 \frac{V'V'''}{V^2},\\ \sigma^3 &\equiv M_{\rm Pl}^6 \frac{V''^2 V^{(4)}}{V^3},\end{aligned} \tag{4.12}$$

that are the third and fourth-order slow-roll parameters in single-field slow-rolling inflation [42](c_s is the adiabatic speed of sound of primordial perurbations).

Running and running of the running are related to the deviations from the scale invariance (i.e. from $n_s = 1$) and for single-field slow-roll inflation we have a prediction of very small values of such deviations, $\mathrm{d}n_s/\mathrm{d}\ln k = \mathcal{O}[(n_s-1)^2] \sim 10^{-3}$ and $\mathrm{d}^2 n_s/\mathrm{d}\ln k^2 = \mathcal{O}[(n_s-1)^3] \sim 10^{-5}$ [37].

The actual value estimated for the running of the spectral index is [17]:

$$\frac{\mathrm{d}n_s}{\mathrm{d}\ln k} = -0.004 \pm 0.015 \qquad (95\%\ \mathrm{CL},\ \textit{Planck}\ \mathrm{TT{+}SIMlow}). \tag{4.13}$$

When we allow also for the running of the running, the constraints from the last 2015 *Planck* data release [25] are:

$$\frac{\mathrm{d}n_s}{\mathrm{d}\ln k} = 0.009 \pm 0.010 \qquad (68\%\ \mathrm{CL},\ \textit{Planck}\ \mathrm{TT,TE,TT{+}lowP}), \tag{4.14}$$

and:

$$\frac{\mathrm{d}^2 n_s}{\mathrm{d}\ln k^2} = 0.025 \pm 0.013 \qquad (68\%\ \mathrm{CL},\ \textit{Planck}\ \mathrm{TT,TE,TT{+}lowP}). \tag{4.15}$$

4.3.1 Contraints for scale dependence parameters

We show now the 68% CL errors obtained considering as fiducial cosmology vanishing runnings. The results obtained for the 7-parameters case are in perfect agreement with the errors from the CORE-M5 analysis, as shown in Tab.4.3, and therefore, as well else for the LCDM, we recover the same results obtained with the MCMC approach. Also in this case the performance by CORE alone will be better in contraining almost the parameters than what Euclid could achieve with the combination with *Planck* data. The

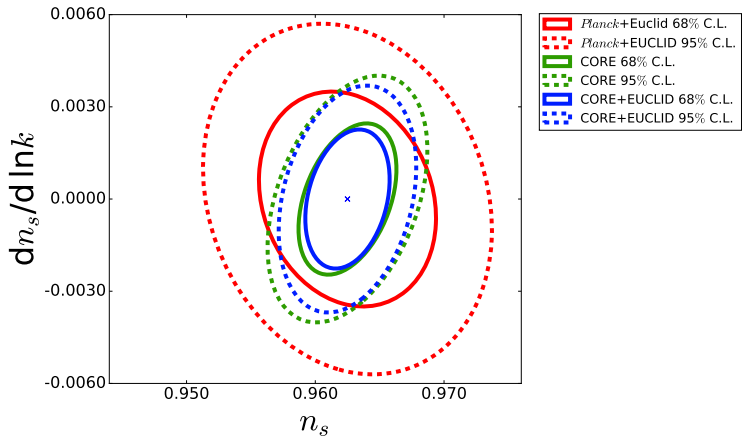

Figure 4.2: Forecast 68% (solid line) and 95% (dashed line) C.L. 2D marginalized regions of the scalar spectral index and its running in a ΛCDM+$\mathrm{d}n_s/\mathrm{d}\ln k$ for CORE (green), CORE+Euclid (blue) and *Planck*+Euclid.

combination of CORE+Euclid lowers the parameter uncertainties even more, showing that their joint contribution will be very helpful in the prediction of inflationary models. In Fig.4.2 we can see how the combination of the LSS and CMB observables helps to break the degeneracies between the spectral index and its running.

In the 8-parameters model, while most of the standard parameter errors show a trend like the ones in the model with only the running of the spectral index, the errors related to the running of the running of the spectral index seems much more sensible to the Euclid contribution, reaching values $\sim 50\%$ lower than one found in our CORE analysis and in CORE-M5. We have checked this particular result in two ways. First we have repeated our analysis after generating LSS data negleting the non-linear evolution, discovering that the error for $\mathrm{d}^2 n_s/\mathrm{d}\ln k^2$ in the Euclid-combined cases rise up to the usual value of $\sim 0.004 - 0.005$ for CORE and of ~ 0.008 for *Planck*. Then we have used again our non-linear data, but considering the contribution of the galaxy clustering power spectra only up to $k_{\mathrm{max}} = 0.1\,h/\mathrm{Mpc}$, where we

have supposed the non-linear contribution would be weaker. We have found no significant deviations from the results obtained with $k_{\rm max} = 0.2\,h/{\rm Mpc}$. We have compared the derivatives of the scale dependence parameters calculated from our non-linear data, reported in Fig.3 of Appendix A, with the ones from our linear data and from linear data showed in Fig.1 on Muñoz et al. [42]. The linear case have shown very similar trends, while they was

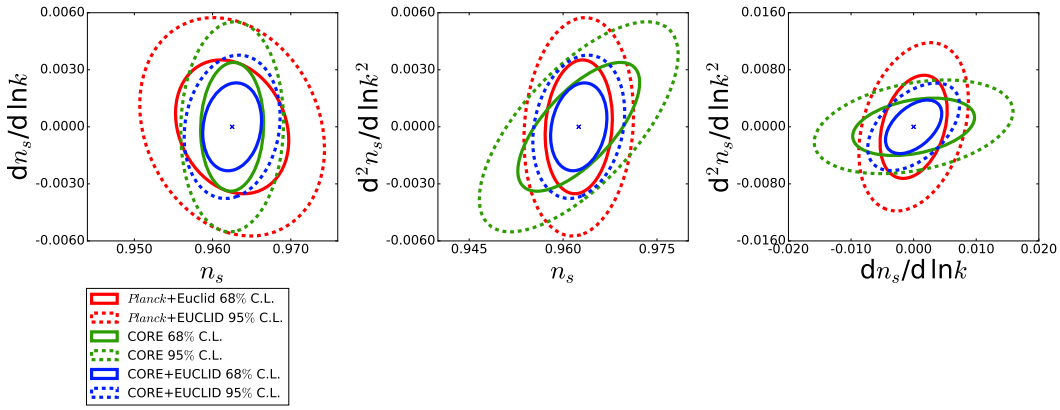

Figure 4.3: Forecast 68% (solid line) and 95% (dashed line) CL 2D marginalized regions of the scalar spectral index and its scale dependence parameters in a ΛCDM+$\mathrm{d}n_s/\mathrm{d}\ln k$+$\mathrm{d}^2n_s/\mathrm{d}\ln k^2$ for CORE (green), CORE+Euclid (blue) and *Planck*+Euclid (red).

slightly different from non-linear ones.

The inclusion of non-linear evolution implies little changes in the features of the derivatives in the range from $k \sim 0.01 - 0.1\,h/{\rm Mpc}$ but, while this mean only an horizontal shift in the running derivative, for the running of the running derivative there is a lowering of the derivative value, keeping it negative and with an higher absolute value up to $k > 0.2\,h/{\rm Mpc}$. All this could mean that the scale dependence parameters are much sensible to non-linear scales, making the improvement achievable with Euclid a key point in the future measure of these parameters. In Fig.4.3 we can see how the combination of the LSS and CMB observables help to break degeneracies in

ΛCDM+dn_s/d ln$k$							
	CORE		CORE-M5 (MCMC)	CORE+Euclid		*Planck*+Euclid	
	T,E	T,E,ϕ	T,E+$\phi\phi$	T,E+$\mathcal{P}(k)$	T,E,ϕ+$\mathcal{P}(k)$	T,E+$\mathcal{P}(k)$	T,E,ϕ+$\mathcal{P}(k)$
$10^6\,\sigma(\omega_b)$	42 [0.019]	40 [0.018]	44 [0.0020]	40 (0.95)	39 (0.98)	110 (2.62)	110 (2.75)
$10^5\,\sigma(\omega_c)$	65 [0.0054]	27 [0.0022]	28 [0.0023]	25 (0.38)	19 (0.70)	35 (0.54)	33 (1.22)
$10^2\,\sigma(H_0)$	25 [0.0037]	11 [0.0016]	11 [0.0016]	9,5 (0.38)	7,4 (0.67)	12 (0.48)	11 (1.00)
$10^4\,\sigma(\tau)$	20 [0.034]	19 [0.033]	20 [0.0344]	19 (0.95)	16 (0.84)	38 (1.90)	36 (1.89)
$10^4\,\sigma(n_s)$	19 [0.0020]	16 [0.0017]	16 [0.0017]	16 (0.84)	15 (0.94)	23 (1.21)	23 (1.44)
$10^4\,\sigma\left(\ln(10^{10}A_s)\right)$	44 [0.0014]	36 [0.0012]	36 [0.0012]	41 (0.93)	31 (0.86)	79 (1.80)	74 (2.06)
$10^4\,\sigma\left(\mathrm{d}n_s/\mathrm{d}\ln k\right)$	25 [-]	24 [-]	24 [-]	22 (0.88)	22 (0.92)	42 (1.68)	42 (1.75)
[*]: relative error (*): ratio with respect to CORE $\sigma(\theta_i)$							
$[H_0]$=[km/s/Mpc] T,E: TT+EE+TE ; T,E,P: TT+EE+TE+$\phi\phi$+Tϕ ; $\mathcal{P}$: $\widetilde{\mathcal{P}}_{\rm obs}$							

Table 4.3: Parameter errors (68% CL) for the extended model ΛCDM+dn_s/d ln$k$ cosmology. We report the MCMC forecasts for CORE-M5 experimental configuration, from Tab.5 of [36].

ΛCDM+dn_s/d ln$k$+d^2n_s/d lnk^2							
	CORE		CORE-M5 (MCMC)	CORE+Euclid		*Planck*+Euclid	
	T,E	T,E,ϕ	T,E+$\phi\phi$	T,E+$\mathcal{P}(k)$	T,E,ϕ+$\mathcal{P}(k)$	T,E+$\mathcal{P}(k)$	T,Eϕ+$\mathcal{P}(k)$
$10^6\,\sigma(\omega_b)$	43 [0.019]	40 [0.018]	44 [0.020]	40 (0.93)	39 (0.98)	110 (2.56)	110 (2.75)
$10^5\,\sigma(\omega_c)$	70 [0.0058]	27 [0.0022]	32 [0.0027]	28 (0.40)	20 (0.74)	37 (0.53)	36 (1.33)
$10^2\,\sigma(H_0)$	27 [0.000]	11 [0.0016]	13 [0.0019]	11 (0.41)	7.7 (0.70)	13 (0.48)	12 (1.09)
$10^4\,\sigma(\tau)$	21 [0.036]	19 [0.033]	21 [0.036]	20 (0.95)	16 (0.84)	38 (1.81)	36 (1.89)
$10^4\,\sigma(n_s)$	28 [0.0029]	21 [0.0022]	22 [0.0023]	17 (0.61)	15 (0.71)	23 (0.82)	23 (1.10)
$10^4\,\sigma\left(\ln(10^{10}A_s)\right)$	51 [0.0017]	37 [0.0012]	40 [0.0013]	43 (0.84)	31 (0.84)	80 (1.57)	75 (2.03)
$10^4\,\sigma\left(\mathrm{d}n_s/\mathrm{d}\ln k\right)$	25 [-]	24 [-]	24 [-]	23 (0.92)	23 (0.96)	42 (1.68)	42 (1.75)
$10^4\,\sigma\left(\mathrm{d}^2n_s/\mathrm{d}\ln k^2\right)$	52 [-]	45 [-]	46 [-]	28 (0.54)	25 (0.56)	31 (0.60)	31 (0.69)
[*]: relative error (*): ratio with respect to CORE $\sigma(\theta_i)$							
$[H_0]$=[km/s/Mpc] T,E: TT+EE+TE ; T,E,P: TT+EE+TE+$\phi\phi$+Tϕ ; $\mathcal{P}$: $\widetilde{\mathcal{P}}_{\rm obs}$							

Table 4.4: Parameter errors (68% CL) for the extended model ΛCDM+dn_s/d ln$k$+d^2n_s/d lnk^2 cosmology. We report the MCMC forecasts for CORE-M5 experimental configuration, from Tab.6 of [36].

scale dependence parameters, specially between dn_s/d ln$k$ and d^2n_s/d lnk^2. For what concerns the slow-roll parameters, the precision achievable with all these future surveys won't be sufficient to detect the prediction of the

single-field slow-roll inflation, but only to measure significant deviations from it. This arises because, despite that the precision achieved for $\mathrm{d}n_s/\mathrm{d}\ln k$ is nearly to appreciable values $\sim 2 \cdot 10^{-3} \gtrsim \mathcal{O}[(n_s - 1)^2]$, the one relative to $\mathrm{d}^2 n_s/\mathrm{d}\ln k^2$ is $\sim 3 \cdot 10^{-3} \gg \mathcal{O}[(n_s - 1)^3]$.
In Muñoz et al. are reported results for the running of the running that are compatible with ours, from the joint forecasts of proposed cosmic surveys such as the Stage-4 (S4) CMB experiment, the Square Kilometer Array extension (SKA2) spectroscopic survey with one billion objects and the Fast Fourier Transform Telescope (FFTT) 21-cm tomography maps. From the combination S4+SKA2 they report a 68% CL uncertainties 0.0020 for the running of the running and 0.0017 from S4+FFTT. Moreover, they show nearly identical results from *Planck*+SKA2 and *Planck*+FFTT. Apart from these result, it is interesting to note that they also considered an ultra-futuristic experiment, a scaled-up lunar FFTT with a 300-km baseline, reporting uncertainties $< 10^{-6}$ for both the runnings from the combination S4+FFTT_{300}, small enough to test single-field slow-roll predictions.
This therefore means that, while the measure of the running at the level of single-field slow-roll prediction will be near the possibilities of the combination of future surveys, the measure of the running of the running will be out of reach for next generation experiments. Nevertheless, the combination of different informations from small-scale observations, such as the weak lensing or the 21-cm emission, will be of fundamental importance.

4.4 Neutrino physics

In the Standard Model of particle physics there are three species of Neutrinos (electron, muon and tau neutrino), electrically neutral fermion particles with a predicted rest mass equal to zero.
They interact only through weak and gravitational forces, but the former has a very short range and the latter is extremely weak on the subatomic scales. These characteristics have made neutrinos, in the past, a suitable candidate

for dark matter particles (both as cold or even warm component). Nevertheless, a little percentage of the DM content of the Universe is attributed to neutrinos.

4.4.1 Cosmic neutrino background

In the early phases of the Universe neutrinos are coupled and in thermal equilibrium with the radiation through scattering interactions. When the rate of these interactions falls below the expansion rate, neutrinos decouple at $T_{\nu,\mathrm{dec}} \simeq 1\,\mathrm{MeV}$, then the neutrino "gas" expands adiabatically with the relation:

$$T_\nu = T_{\nu,\mathrm{dec}} \frac{a(t_{\mathrm{dec}})}{a}. \tag{4.16}$$

The radiation temperature T_γ evolves following the same law but at the electron-positron annihilation it is slightly increased due to the energy density transfered. This can be shown by imposing conservation of entropy density at the annihilation, that is always around $T \sim 1\,\mathrm{MeV}$. In radiation dominated epochs we have an entropy density:

$$s = \frac{2\,\pi^2}{45} g_*(T) T^3, \tag{4.17}$$

where $g_*(T)$ is the effective number of degrees of freedom, considering all the particles in thermal equilibrium:

$$g_* \equiv \sum_{bosons} g_*^i + \frac{7}{8} \sum_{fermions} g_*^i. \tag{4.18}$$

Entropy conservation implies $g_*^{(-)} T_{(-)}^3 = g_*^{(+)} T_{(+)}^3$, where $(-)$ and $(+)$ denote the quantities before and after a pair annihilation. When electrons, positrons and photons are in thermal equilibrium $g_*^{(-)} = 11/2$. After the annihilation only photons are termalized, therefore $g_*^{(+)} = 2$. The result is that:

$$T_\gamma = T_{(+)} = \left(\frac{11}{4}\right)^{1/3} T_{(-)} \simeq 1.4\, T_{(-)} = 1.4\, T_\nu, \tag{4.19}$$

with which one finds that $T_{0,\nu} \simeq 0.7\, T_{0,\gamma} \simeq 1.95\,\mathrm{K}$. The neutrino number density is then:

$$n_{0,\nu} = 2\, g_\nu N_\nu \frac{3}{4} \frac{\zeta(3)}{\pi^2} \left(\frac{k_B T_{0,\nu}}{\hbar\, c} \right)^3, \tag{4.20}$$

where ζ is the Riemann Zeta function ($\zeta(3) \simeq 1.202$ is also called Apéry's constant), corresponding to a value $n_{0,\nu} \simeq N_\nu\, 108\,\mathrm{cm}^{-3}$. The present energy density of neutrinos depends on whether they are relativistic or not today. For relativistic neutrinos at epochs $T \ll 1\,\mathrm{MeV}$, we have:

$$\rho_\nu = N_{\mathrm{eff}} \frac{7}{8} \left(\frac{4}{11} \right)^{4/3} \rho_\gamma. \tag{4.21}$$

where N_{eff} is the effective number of neutrinos. For three thermalized standard model neutrinos instantaneously decoupled we have $N_{\mathrm{eff}} = 3$. The correct prediction from standard cosmology is actually $N_{\mathrm{eff}} \simeq 3.046$, since neutrinos are not completely decoupled from radiation during the electron-positron annihilation [29]. Since $\rho_{\gamma,0} \sim 10^{-5}$, we therefore have for relativistic (or massless) neutrinos that $\omega_\nu^{\mathrm{rel}} \simeq 1.7 \cdot 10^{-5}$.

Experimental evidences of neutrino oscillations imply that neutrinos have masses. This results have earned the Nobel Prize in Physics for 2015 to Takaaki Kajita [27] (Super-Kamiokande Collaboration) and Arthur B. McDonald [28] (Sudbury Neutrino Observatory Collaboration). Considering the value of neutrino number density and their massive nature, their masses have to be extremely small. In order to have $\Omega_\nu < 1$, we can see that from $\rho_\nu = n_\nu \langle \sum m_\nu \rangle$ it follows that $\sum m_\nu < 15\,\mathrm{eV}$. With such masses the neutrinos should be non-relativistic at present time. The physical energy density for massive neutrinos is actually parametrized as $\omega_\nu \simeq \sum m_\nu / 94\,\mathrm{eV}$.

4.4.2 Impact of neutrino properties on Cosmology

Neutrino properties have an important role in both early and late stages of our universe. Massive neutrinos have an impact on the background expansion history, influencing the value of the redshift of matter-Λ equivalence and

before the late-ISW effect. Massive neutrinos also interact gravitationally and they can have an impact on the CMB peaks (high-ℓ tail) and influence the early-ISW. For the same reason, they can also have an impact the BAO. Furthermore, they could slow down the growth of smaller structure, globally decreasing the impact of CMB lensing [38].
Deviations from the standard number of degrees of freedom due to additional contributions $N_{\rm eff} > 3.046 \Rightarrow \Delta N_{\rm eff} > 0$ could arise, for instance, from having a non-zero amount of extra-relativistic relics or dark radiation (a postulate type of radiation that mediates interactions of DM and for which a possible candidate is the sterile neutrino [30]) or if the radiation has a non-termic counterpart non fully thermalized because of particle decays [31]. Values of $\Delta N_{\rm eff} < 0$ are less well motivated, because it would required non-fully thermalized standard neutrinos or additional photon procution after neutrino decoupling, but they can be nevertheless considered.
The actual constrains on the number of relativistic species in a ΛCDM+$N_{\rm eff}$ model with three neutrinos, always referring to [17], is:

$$N_{\rm eff} = 2.97^{+0.58}_{-0.53} \qquad (95\%\ \text{CL, } \textit{Planck}\ \text{TT+SIMlow}), \tag{4.22}$$

It is possible to use cosmological data to constrain neutrino mass. One approach is to consider two massless neutrinos and fixing the total mass to the minimal value allowed from oscillation experiments. An other is to consider three degenerate neutrinos, a good approximation as long as the total mass is much higher than the minimal value. Both the two approaches are only approximations, but since oscillations measurements provide information only on the splittings between the three mass eigenstates, we don't have independent information on their total mass value nor their hierarchical structure [32]. For these reasons, the two approaches mentioned are used being the limit cases respectively of the hierarchy assumption $m_1 \lesssim m_2 \ll m_3$ and of the degenerate one $m_1 \lesssim m_2 \lesssim m_3$. The former is also called normal hierarchy , in order to distinguish it from the inverse hierarchy $m_1 \ll m_2 \lesssim m_3$ (hereafter with we will refer only to the normal case).
The hierarchical model generally assumes a total neutrino mass $\sum m_\nu \approx$

0.06 eV, dominated by the heaviest netrino mass eigenstate, while the degenerate model includes the possibility of values $\sum m_\nu \gtrsim 0.1\,\mathrm{eV}$ [26].
The actual upper limit estimation for the neutrino total mass, referred to [17], in a ΛCDM+$\sum m_\nu$ model with three massive neutrinos is:

$$\sum m_\nu < 0.585\,[\mathrm{eV}] \qquad (95\%\ \mathrm{CL},\ \textit{Planck}\ \mathrm{TT+SIMlow}), \tag{4.23}$$

It is useful to investigate also models that afford us to get simultaneous constraints on $\sum m_\nu$ and N_{eff}, considering $N_{\mathrm{eff}} = N_\nu + N_{\mathrm{eff}}^{\mathrm{rel}}$, where N_ν denotes the number of massive neutrinos.

4.4.3 Constraints for neutrino masses and relativistic species

We have analysed five scenarios concerning neutrinos, for all of which we have assumed three neutrinos and an effective number $N_{\mathrm{eff}} = 3.046$.
First, we have considered the extended ΛCDM+$N_{\mathrm{eff}}^{\mathrm{rel}}$ model for massless neutrinos in which we vary the effective number of relativistic species around the fiducial value $N_{\mathrm{eff}}^{\mathrm{rel}} = 3.046$.
Then we have examined the two limit scenarios for massive neutrinos, i.e. the three massive degenerate and the one massive-two massless hierarchical models. We assume for both of the extended ΛCDM+$\sum m_\nu$ cosmology a fiducial value $\sum m_\nu = 0.06\,\mathrm{eV}$, where the mass for the degenerate case is equally splitted.
We have also considered the two extended ΛCDM+$\sum m_\nu$+$N_{\mathrm{eff}}^{\mathrm{rel}}$ models with fiducial values respectively $N_{\mathrm{eff}}^{\mathrm{rel}} = 0.046$ for the degenerate case and $N_{\mathrm{eff}}^{\mathrm{rel}} = 2.046$ for the hierarchical one. From a general point of view, all the results are quite in agreement with other references [33, 38, 32] and the improvement reached with CORE gives better results with respect to *Planck*+Euclid for most of the parameters. The contribution of Euclid is very helpful in contraining parameters such as ω_c and H_0, for which the information from LSS observables helps to break parameter degeneracies and it is essential for the

ΛCDM+$N_{\rm eff}^{\rm rel}$ ($N_\nu = 0$)							
	CORE		CORE-M5 (MCMC)	CORE+Euclid		*Planck*+Euclid	
	T,E	T,E,ϕ	T,E+$\phi\phi$	T,E+$\mathcal{P}(k)$	T,E,ϕ+$\mathcal{P}(k)$	T,E+$\mathcal{P}(k)$	T,E,ϕ+$\mathcal{P}(k)$
$10^6\,\sigma(\omega_b)$	54 [0.024]	53 [0.024]	47 [0.0021]	40 (0.74)	37 (0.70)	94 (1.74)	94 (1.77)
$10^5\,\sigma(\omega_c)$	91 [0.0075]	61 [0.0051]	+52 [0.0043]/−74 [0.0062]	72 (0.79)	47 (0.77)	120 (1.32)	110 (1,80)
$10^2\,\sigma(H_0)$	42 [0.0063]	34 [0.0051]	+71 [0.011]/−50 [0.0074]	14 (0.33)	13 (0.38)	17 (0.40)	17 (0.50)
$10^4\,\sigma(\tau)$	20 [0.034]	19 [0.033]	21 [0.035]	19 (0.95)	17 (0.89)	37 (1.85)	36 (1.89)
$10^4\,\sigma(n_s)$	30 [0.0031]	26 [0.0027]	23 [0.0024]	17 (0.57)	16 (0.62)	23 (0.77)	23 (0.88)
$10^4\,\sigma\left(\ln(10^{10}A_s)\right)$	45 [0.0015]	37 [0.0012]	42 [0.0014]	42 (0.93)	28 (0.76)	78 (1.73)	71 (1.92)
$10^3\,\sigma(N_{\rm eff}^{\rm rel})$	47 [0.015]	43 [0.014]	< 40 [-]	30 (0.64)	23 (0.53)	50 (1.06)	48 (1.12)
[*]: relative error (*): ratio with respect to CORE $\sigma(\theta_i)$							
$[H_0]$=[km/s/Mpc] T,E: TT+EE+TE ; T,E,P: TT+EE+TE+$\phi\phi$+Tϕ ; $\mathcal{P}$: $\widetilde{\mathcal{P}}_{\rm obs}$							

Table 4.5: Parameter errors (68% C.L.) for the extended model ΛCDM+$N_{\rm eff}^{\rm rel}$. We report the MCMC forecasts for CORE-M5 experimental configuration, from Tab.6 of [33]

neutrino physics parameters. The combination CORE+Euclid reach an impressive level of precision, thanks to the different information related to CMB and galaxy clustering and in all the cases considered we see improvements in the errors related to $N_{\rm eff}^{\rm rel}$ and/or $\sum m_\nu$, up to $\sim 60 \div 80\%$ lower than ones for CORE alone.

The results of the ΛCDM+$N_{\rm eff}^{\rm rel}$ model in Tab. 4.5 show, despite the massless nature assumed for neutrinos, that there is strong degeneracy between the number of relativistic species and the physical density parameters, but also with the primordial spectrum parameters A_s and n_s. Nevertheless, the uncertainties are in agreement with CORE-M5 data, showing that the combination CORE+Euclid could constrain the neutrino properties related to the effective number of relativistic species.

For what concerns the models with 3 degenerate massive neutrinos, we have compared the results with a similar case in Gerbino et al. [32] and there is a confirmation in the presence of degeneracy between $N_{\rm eff}^{\rm rel}$ and the scalar spectral index, but also with the optical reionization. Moreover, besides the combination of CORE+Euclid, these degeneracies are difficul to be bro-

ken. The error related to the total mass in the 7-parameter case, from the joined information of CMB, LSS and CMB lensing and shown in Tab. 4.6, are enough small to predict $0\,\mathrm{eV} < \sum m_\nu < 0.12\,\mathrm{eV}$ within 5σ for degenerate massive neutrinos, a result compatible with other LSS survey forecasts [43]. In the 8-parameters model, the degeneracy with $N_{\mathrm{eff}}^{\mathrm{rel}}$ reduce this prediction to $\sim 4\sigma$, as shown in Tab. 4.7.

The hierarchical cases show results in agreement with the errors taken from the CORE-M5 analysis. The Fisher method seems to work quite well in giving approximated results for these cases, despite the fact that for parameters like the DM physical density, the Hubble parameter and the total mass the MCMC method reports asymmetric errors, due to the presence of non-Gaussian features in the likelihood. In the ΛCDM+$\sum m_\nu$ the combination of CORE+Euclid helps to break degeneracies in w_c, H_0 and $\sum m_\nu$ parameters. Moreover, the contraints for neutrino total mass open the possibility of verifying their massive nature at more than 5σ, considering the T,E,ϕ+LSS case in Tab. 4.8. In the ΛCDM+$\sum m_\nu$+$N_{\mathrm{eff}}^{\mathrm{rel}}$ this effect is slightly reduced, due to the degeneracy between the neutrino total mass and the number of relativistic species, but it is compatible with the CORE-M5 results shown in Tab. 4.9.

We remind that these results are optimistic, both for the nature of the Fisher approach and because, as it is said in Archidiacono et al. [38], such analysis need the consideration of extra-teoric uncertainties due to the neutrino physics, its impact on the observables and the non-trivial degeneracies that emerge as consequence. Nevertheless, next generation surveys will probably be able to constrain the neutrino masses with high precision and to reveal their hierarchy.

ΛCDM+$\sum m_\nu$ ($N_\nu = 3$)						
	CORE		CORE+Euclid		*Planck*+Euclid	
	T,E	T,E,ϕ	T,E+$\mathcal{P}(k)$	T,E,ϕ+$\mathcal{P}(k)$	T,E+$\mathcal{P}(k)$	T,E,ϕ+$\mathcal{P}(k)$
$10^6\,\sigma(\omega_b)$	37 [0.017]	35 [0.016]	34 (0.92)	33(0.94)	97 (2.62)	97 (2.77)
$10^5\,\sigma(\omega_c)$	65 [0.0054]	53 [0.0044]	42 (0.65)	20 (0.38)	53 (0.82)	47 (0.89)
$10^2\,\sigma(H_0)$	68 [0.010]	54 [0.0081]	9.6 (0.14)	9.6 (0.18)	11 (0.16)	10 (0.19)
$10^4\,\sigma(\tau)$	20 [0.034]	19 [0.033]	19 (0.95)	19 (1.00)	39 (1.95)	39 (2.05)
$10^4\,\sigma(n_s)$	18 [0.0019]	17 [0.0018]	16 (0.89)	14 (0.82)	25 (1.39)	23 (1.35)
$10^4\,\sigma\left(\ln(10^{10}A_s)\right)$	42 [0.0014]	38 [0.0012]	40 (0.95)	35 (0.92)	76 (1.81)	74 (1.95)
$10^3\,\sigma(\sum m_\nu)$	72 [1.2]	41 [0.68]	19 (0.26)	11 (0.27)	24 (0.33)	22 (0.54)
[*]: relative error (*): ratio with respect to CORE $\sigma(\theta_i)$						
$[H_0]$=[km/s/Mpc] $[m_\nu]$=[eV] T,E: TT+EE+TE ; T,E,P: TT+EE+TE+$\phi\phi$+Tϕ ; $\mathcal{P}$: $\widetilde{\mathcal{P}}_{\rm obs}$						

Table 4.6: Parameter errors (68% C.L.) for the extended ΛCDM+$\sum m_\nu$ cosmology with three degenerate massive neutrinos.

ΛCDM+$\sum m_\nu$+$N_{\rm eff}^{\rm rel}$ ($N_\nu = 3$)						
	CORE		CORE+Euclid		*Planck*+Euclid	
	T,E	T,E,ϕ	T,E+$\mathcal{P}(k)$	T,E,ϕ+$\mathcal{P}(k)$	T,E+$\mathcal{P}(k)$	T,E,ϕ+$\mathcal{P}(k)$
$10^6\,\sigma(\omega_b)$	48 [0.022]	47 [0.021]	40 (0.83)	40 (0.85)	100 (2.08)	100 (2.13)
$10^5\,\sigma(\omega_c)$	81 [0.0067]	70 [0.0058]	61 (0.75)	47 (0.67)	87 (1.07)	83 (1.19)
$10^2\,\sigma(H_0)$	71 [0.011]	59 [0.0088]	12 (0.17)	12 (0.20)	14 (0.20)	14 (0.24)
$10^4\,\sigma(\tau)$	20 [0.034]	19 [0.033]	19 (0.95)	19 (1.00)	39 (1.95)	39 (2.05)
$10^4\,\sigma(n_s)$	26 [0.0027]	24 [0.0025]	19 (0.73)	17 (0.71)	26 (1.00)	25 (1.04)
$10^4\,\sigma\left(\ln(10^{10}A_s)\right)$	44 [0.0014]	40 [0.0013]	42 (0.95)	37 (0.93)	79 (1.80)	77 (1.93)
$10^3\,\sigma(\sum m_\nu)$	73 [1.22]	41 [0.68]	21 (0.29)	14 (0.34)	26 (0.36)	24 (0.59)
$10^3\,\sigma(N_{\rm eff}^{\rm rel})$	36 [0.78]	34 [0.74]	26 (0.72)	25 (0.74)	37 (1.03)	37 (1.09)
[*]: relative error (*): ratio with respect to CORE $\sigma(\theta_i)$						
$[H_0]$=[km/s/Mpc] $[m_\nu]$=[eV] T,E: TT+EE+TE ; T,E,P: TT+EE+TE+$\phi\phi$+Tϕ ; $\mathcal{P}$: $\widetilde{\mathcal{P}}_{\rm obs}$						

Table 4.7: Parameter errors (68% C.L.) for the extended ΛCDM+$\sum m_\nu$+$N_{\rm eff}^{\rm rel}$ cosmology with three degenerate massive neutrinos.

ΛCDM+$\sum m_\nu$ ($N_\nu = 1$)							
	CORE		CORE-M5 (MCMC)	CORE+Euclid		*Planck*+Euclid	
	T,E	T,E,ϕ	T,E+$\phi\phi$	T,E+$\mathcal{P}(k)$	T,E,ϕ+$\mathcal{P}(k)$	T,E+$\mathcal{P}(k)$	T,E,ϕ+$\mathcal{P}(k)$
$10^6\,\sigma(\omega_b)$	37 [0.017]	36 [0.016]	39 [0.018]	33 (0.89)	33 (0.92)	95 (2.57)	95 (2.64)
$10^5\,\sigma(\omega_c)$	65 [0.0054]	57 [0.0047]	+43 [0.0036]/−65 [0.0054]	39 (0.60)	19 (0.33)	49 (0.75)	44 (0.77)
$10^2\,\sigma(H_0)$	71 [0.011]	52 [0.0078]	+73 [0.011]/−39 [0.0058]	9.8 (0.14)	9.7 (0.19)	11 (0.15)	11 (0.21)
$10^4\,\sigma(\tau)$	20 [0.034]	19 [0.033]	20 [0.033]	19 (0.95)	19 (1.00)	39 (1.95)	39 (2.05)
$10^4\,\sigma(n_s)$	18 [0.0019]	17 [0.0018]	18 [0.0019]	16 (0.89)	14 (0.82)	24 (1.33)	23 (1.35)
$10^4\,\sigma\left(\ln(10^{10}A_s)\right)$	42 [0.0014]	38 [0.0012]	40 [0.0013]	40 (0.95)	35 (0.92)	76 (1.81)	73 (1.92)
$10^4\,\sigma(\sum m_\nu)$	71 [1.18]	35 [0.58]	+37 [0.51]/−51 [0.71]	17 (0.24)	9.3 (0.27)	20 (0.28)	19 (0.54)
[*]: relative error (*): ratio with respect to CORE $\sigma(\theta_i)$							
$[H_0]$=[km/s/Mpc] $[m_\nu]$=[eV] T,E: TT+EE+TE ; T,E,P: TT+EE+TE+$\phi\phi$+Tϕ ; $\mathcal{P}$: $\widetilde{\mathcal{P}}_{\rm obs}$							

Table 4.8: Parameter errors (68% C.L.) for the extended model ΛCDM+$\sum m_\nu$ cosmology with one massive and two massless neutrinos. We report the MCMC forecasts for CORE-M5 experimental configuration, from Tab.12 of [33].

ΛCDM+$\sum m_\nu$+$N_{\rm eff}^{\rm rel}$ ($N_\nu = 1$)							
	CORE		CORE-M5 (MCMC)	CORE+Euclid		*Planck*+Euclid	
	T,E	T,E,ϕ	T,E+$\phi\phi$	T,E+$\mathcal{P}(k)$	T,E,ϕ+$\mathcal{P}(k)$	T,E+$\mathcal{P}(k)$	T,E,ϕ+$\mathcal{P}(k)$
$10^6\,\sigma(\omega_b)$	54 [0.024]	53 [0.024]	60 [0.0027]	46 (0.85)	45 (0.85)	100 (1.85)	100 (1.89)
$10^5\,\sigma(\omega_c)$	92 [0.0076]	86 [0.0071]	77 [0.0064]	74 (0.80)	67 (0.78)	13 (1.41)	13 (1.51)
$10^2\,\sigma(H_0)$	74 [0.011]	58 [0.0087]	+76 [0.011]/−58 [0.0087]	14 (0.19)	14 (0.24)	19 (0.26)	19 (0.33)
$10^4\,\sigma(\tau)$	20 [0.034]	19 [0.033]	21 [0.035]	20 (1.00)	19 (1.00)	39 (1.95)	39 (2.05)
$10^4\,\sigma(n_s)$	30 [0.0031]	27 [0.0028]	30 [0.0031]	21 (0.70)	19 (0.70)	28 (0.93)	27 (1.00)
$10^4\,\sigma\left(\ln(10^{10}A_s)\right)$	45 [0.0015]	42 [0.0014]	45 [0.0015]	43 (0.96)	39 (0.93)	85 (1.89)	82 (1.95)
$10^4\,\sigma(\sum m_\nu)$	72 [1.2]	35 [0.58]	+37 [0.51]/−52 [0.71]	20 (0.28)	14 (0.40)	26 (0.36)	25 (0.71)
$10^4\,\sigma(N_{\rm eff}^{\rm rel})$	47 [0.023]	44 [0.022]	41 [0.013]	37 (0.79)	36 (0.82)	68 (1.45)	68 (1.55)
[*]: relative error (*): ratio with respect to CORE $\sigma(\theta_i)$							
$[H_0]$=[km/s/Mpc] $[m_\nu]$=[eV] T,E: TT+EE+TE ; T,E,P: TT+EE+TE+$\phi\phi$+Tϕ ; $\mathcal{P}$: $\widetilde{\mathcal{P}}_{\rm obs}$							

Table 4.9: Parameter errors (68% C.L.) for the extended model ΛCDM+$\sum m_\nu$+$N_{\rm eff}^{\rm rel}$ cosmology with one massive and two massless neutrinos. We report the MCMC forecasts for CORE-M5 experimental configuration, from Tab.7 of [33].

Appendix A

Numerical derivatives

In Chapter 3 we have introduced the numerical approximation with wich we have calculated the partial derivatives of the power spectra with respect to the parameters of the model, i.e. the symmetric difference quotient:

$$\frac{f(\theta_i + \Delta_i) - f(\theta_i - \Delta_i)}{2\Delta_i} \approx \left.\frac{\partial f(\theta)}{\partial \theta_i}\right|_{\theta_0}, \tag{A.1}$$

that numerically approximates symmetric derivative. The stability check has been done comparing different steps with also the five-point stencil formula, that is:

$$\frac{-f(\theta_i + 2\,\Delta_i) + 8\,f(\theta_i + \Delta_i) - 8\,f(\theta_i - \Delta_i) + f(\theta_i - 2\,\Delta_i)}{12\Delta_i} \approx \left.\frac{\partial f(\theta)}{\partial \theta}\right|_{\theta_0}. \tag{A.2}$$

We have choise the steps ϵ in order to have a percentage spacing $\Delta_i = \epsilon\theta_i$, a part for that parameters with fiducial value equal to zero, for wich the spacing was absolute $\Delta_i = \epsilon$. The checked steps are $\epsilon = 3 \cdot 10^{-1}, 3 \cdot 10^{-2}, 3 \cdot 10^{-3}$. We have verified that the combination of the approximation in Eq. (A.1) with a step of $3 \cdot 10^{-2}$ gives results with appreciable stability.
We have observed what follows:

- parameters for which $\Delta_i = \epsilon\theta_i$ have shown most of the time similar results for both the derivative methods and for the different steps;

- some results for $\epsilon = 3 \cdot 10^{-1}$ were too raw approximations, unable to capture the most variable features, while others for $\epsilon = 3 \cdot 10^{-3}$ have shown spurious fluctuations due to the computational limits (i.e. the discrete nature of the datasets);

- derivative stability have shown a higher dependence for the chosen step than for the numerical method ,with consequent similar results for Eq. (A.1) and Eq. (A.2) .

We report in the following figure the derivative results used in our analysis and an example of the comparison between different methods and step choices.
In Fig. A.1 we listed the plots for the derivatives $\partial C_\ell^X / \partial \theta_i$ for the ΛCDM parameters. Virtually all the derivatives show regular shapes with a good level of smoothness. The only exception is $\partial C_{\phi\phi}^X / \partial \tau$, in which we can observe an example of spurious fluctuations. This is due to the fact that the CMB lensing potential do not have any dependence on the reionization optical depth. Consequently, we have directly set this derivative term equal to zero during the Fisher analysis.
In Fig. A.2 we listed the plots for the derivatives $\partial C_\ell^X / \partial \theta_i$ for the extra parameters in our model. Also in this case most the derivatives have a regular behavior. For what concern the irregularities present in some of the neutrino masses and relativistic species parameter derivatives, we have checked both that they was the best option between the different methods used and that those fluctuations was still acceptable.
In Fig. A.3 we listed the plots for the derivatives $\partial \mathcal{P}_m(\bar{z}_j) / \partial \theta_i$ for both the ΛCDM and extra parameters for each redshift bin centered in $\bar{z}_j$. Here the considerations are the same of the previous cases. The DM density field power spectra have no dependence on parameter τ, so we have set the derivatives with respect to it equal to zero.

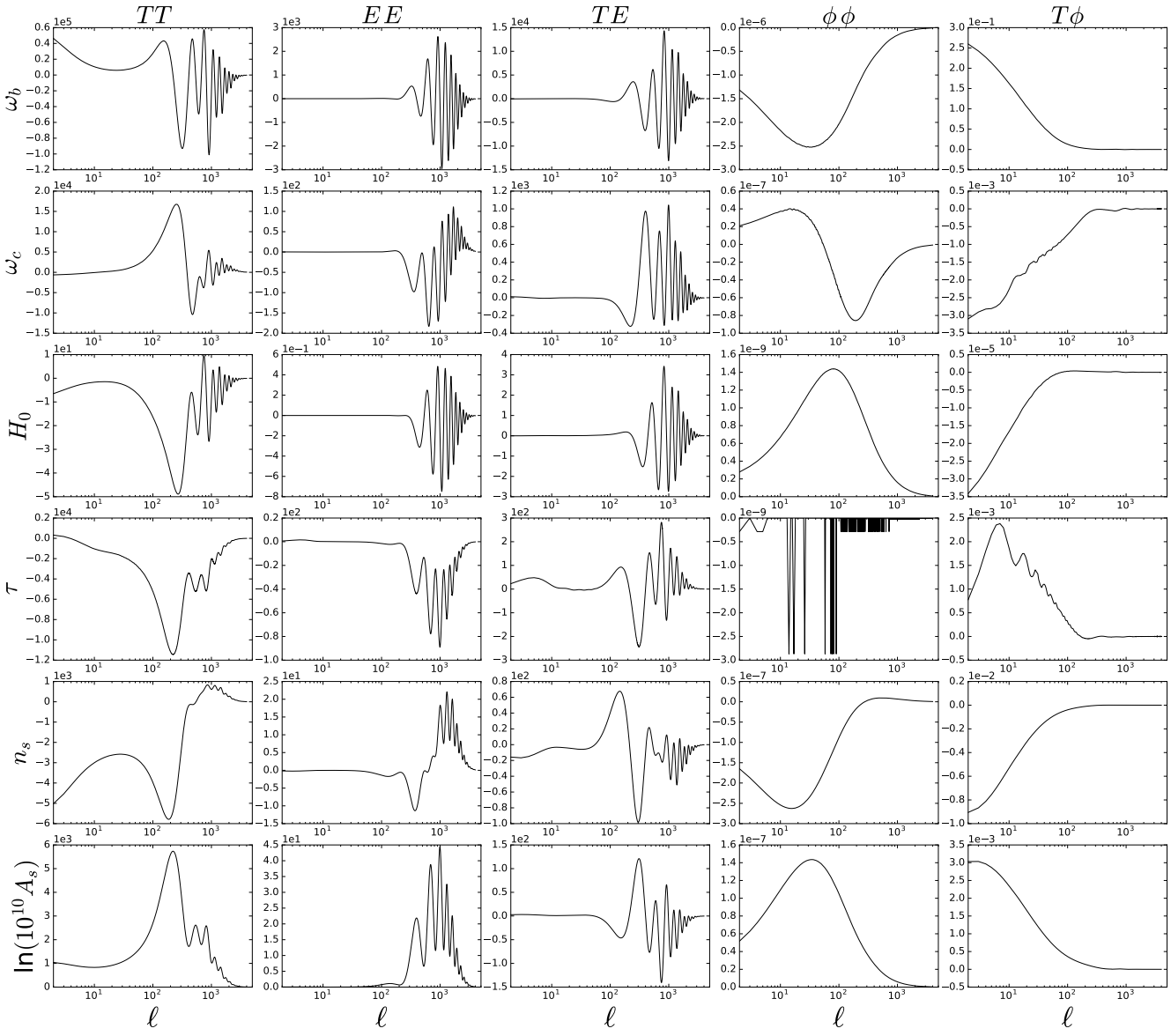

Figure A.1: Numerical derivatives of CMB angular power spectra C_l^X, with respect to the ΛCDM parameters.

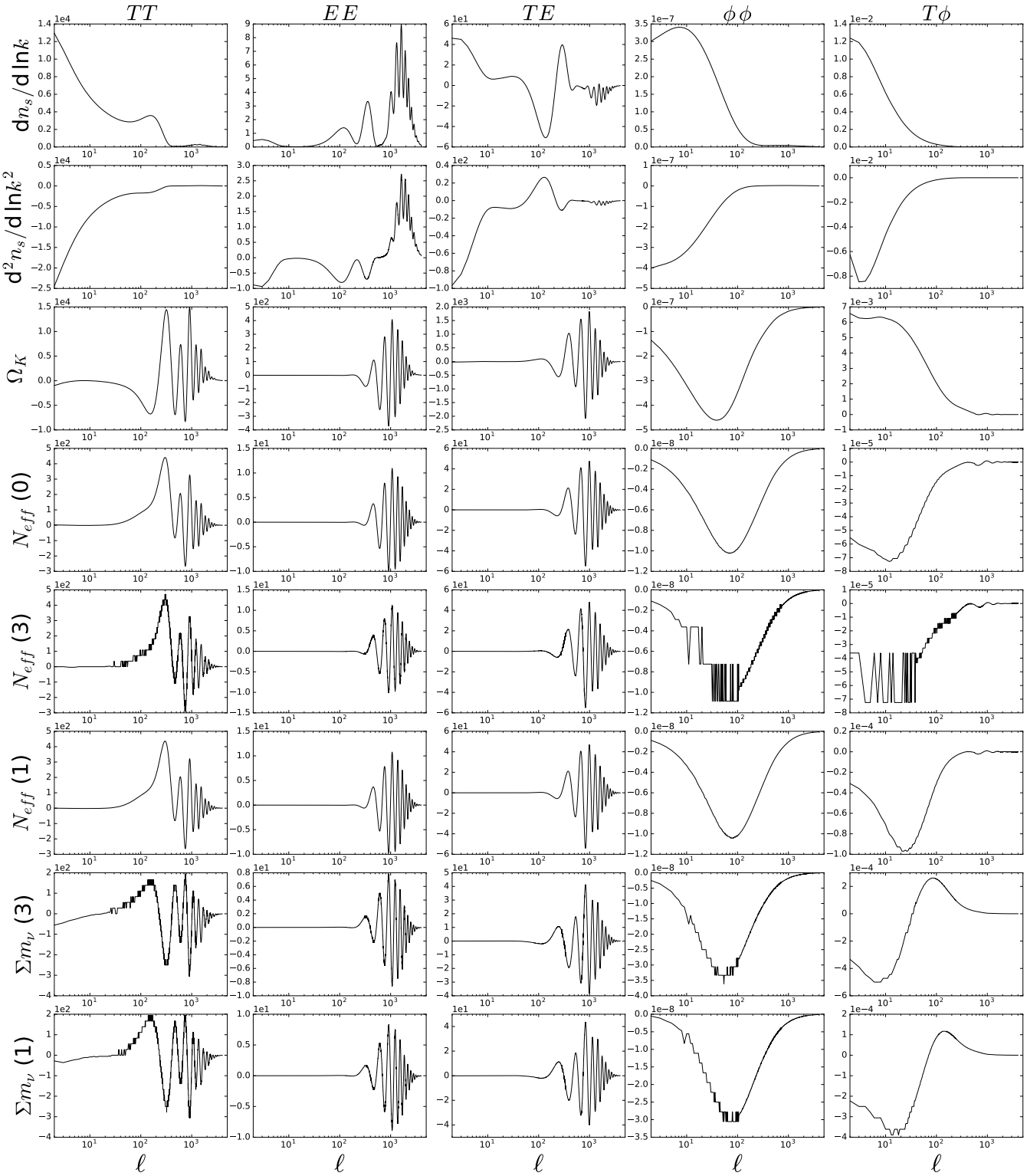

Figure A.2: Numerical derivatives of CMB angular power spectra C_l^X, with respect to the extra parameters. The numbers in bracked refers to the number of massive neutrinos in the models.

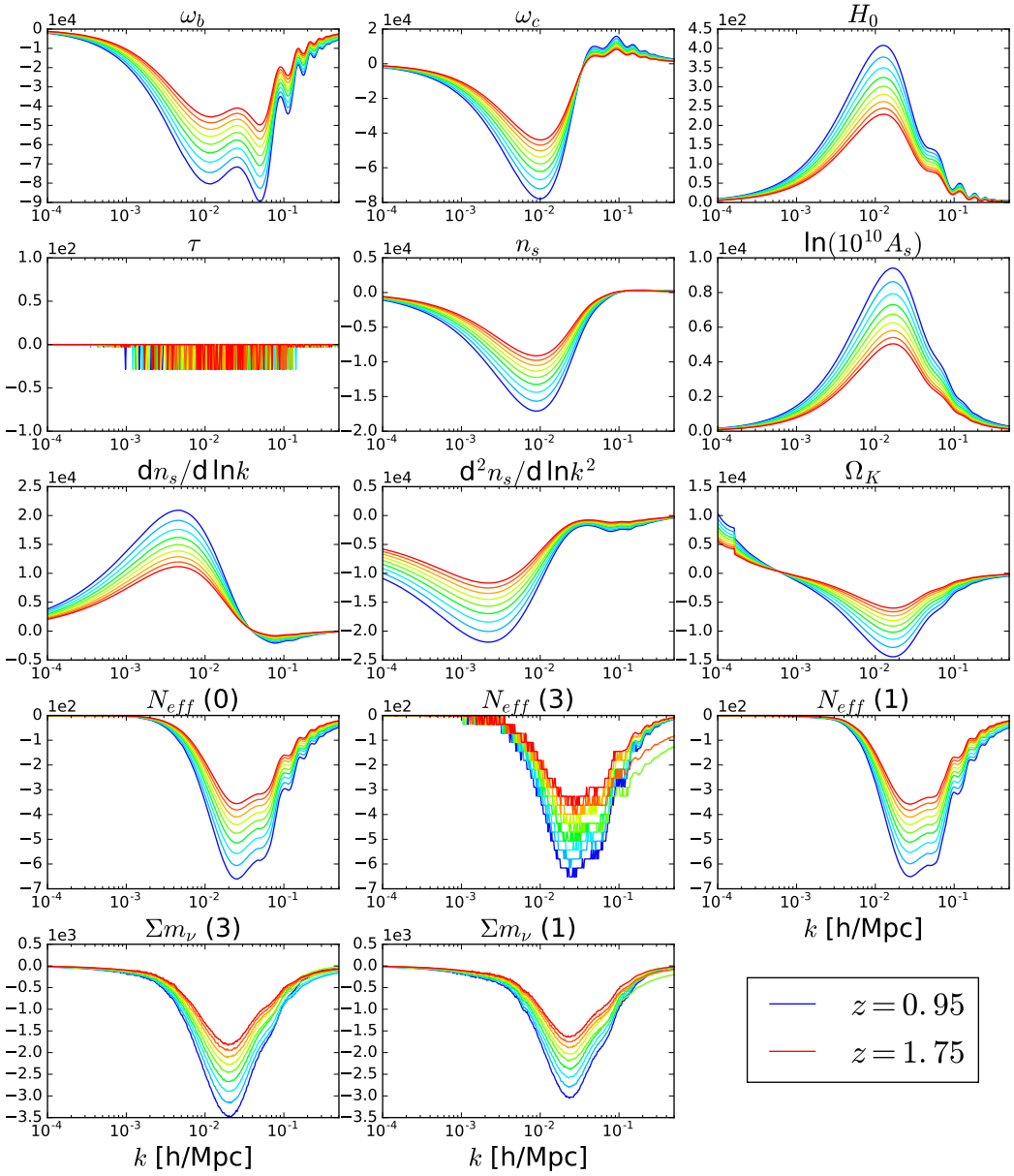

Figure A.3: Numerical derivatives of dark matter density field power spectra $\mathcal{P}_m(k)$, with respect to all the parameters considered. The numbers in bracked refers to the number of massive neutrinos in the models.

Conclusions

In this thesis we have forecasted the uncertainties for cosmological parameters achievable by CORE, a proposed CMB satellite submitted in October 2016 in response to the ESA M5 call for a medium-size mission opportunity. We have combined the CMB anisotropies simulated for CORE with the simulated galaxy clustering power spectrum expected for the Euclid spectroscopic survey, in order to test the capabilities of the combination of CMB and LSS in breaking the parameter degeneracies and improve the constraints on cosmological parameters. We have compared these joint forecasts with ones obtained with the *Planck*+Euclid combination, in order to assess the improvement led by CORE in the post-Euclid era.

We have adopted the Fisher information matrix approach for the forecasts analysis, that assumes a Gaussian approximation of the likelihood.

We have forecasted the uncertainties in the cosmological parameters for the standard ΛCDM model and for several possible extensions. For extended models with an extra parameter we have considered the spatial curvature density parameter Ω_K, the running $\mathrm{d}n_s/\mathrm{d}\ln k$, the number of relativistic species $N_{\rm eff}$ and the total neutrino mass $\sum m_\nu$.

We have also studied extended models with two extra parameters, such as scale dependence wich also allows $\mathrm{d}^2 n_s/\mathrm{d}\ln k^2$ and a more general neutrino sector with both $N_{\rm eff}$ and $\sum m_\nu$ allowed to vary.

As a byproduct of this work, we have tested the reliability of the Fisher matrix approach in forecasting the uncertainties of cosmological parameters in different models, comparing our constraints with the public results obtained

with a Markov Chain Monte Carlo (MCMC) approach. In particular, we found that the results obtained for the ΛCDM model are in agreement with the MCMC forecasts. Fisher information methodology can therefore be used as an alternative to MCMC methods to predict the constraints on cosmological parameters in ΛCDM model, giving reliable forecasts with an appreciable simplification of the method and a reduction of the computational time.

As already reported in the literature, larger differences between the Fisher approach and MCMC are found for ΛCDM+$\sum m_\nu$ [12, 8].

As highlights of our analysis we report that the CORE uncertainties are, in most of the cases, smaller than those for Planck+Euclid. The accuracy level achieved with the combination of CORE+Euclid information makes possible to further reduce the expected uncertainties obtained for CORE of about $10 - 30\%$ for most of the six ΛCDM parameters.

The joint forecasts for extended models with a scale dependence of the spectral index has shown that CORE+Euclid can improve less than 10% the CORE alone result, getting closer to the prediction of single-field slow-roll inflation, $\sim 2 \cdot 10^{-3} \gtrsim \mathcal{O}[(n_s - 1)^2] \simeq 10^{-3}$. The improvement due to the combination with Euclid is about 40% for the running of running, but still far from the possibility to measure the slow-roll prediction, being $\sim 3 \cdot 10^{-3} \gg \mathcal{O}[(n_s - 1)^3] \simeq 10^{-5}$.

In the ΛCDM+$N_{\rm eff}^{\rm rel}$ CORE alone gives lower contraints on the number of relativistic particles with respect to *Planck*+Euclid, and its combination with Euclid strongly reduces the error on $N_{\rm eff}^{\rm rel}$,.

Our results from the combination of CORE and Euclid shows a constraint of the neutrino total mass at more than 5σ. Although these results are optimistic, both because Fisher approach provide idealistic uncertainties and we have neglected theoretical uncertainties on non-linear scales on the matter power spectrum that are related to the neutrino mass, they suggest that constraining the neutrino masses with high precision and revealing what kind of hierarchy they have will be attainable results from future surveys.

In the future the work will be extended in several directions. We will consider

other models, for instance in the analysis of primordial fluctuations we will include also the tensor modes. Moreover, the current result can be further combined with the Euclid weak lensing likelihood. We will consider other surveys in order to make a comparison between different technical specifications and observables involved. Comparison of the Fisher approach with other more computationally heavy will provide information on the reliability of this approach and determine when it can be used to save computational time.

Bibliography

[1] A. R. Liddle and D. H. Lyth, *Cosmological Inflation and Large-Scale Structure*, Cambridge University Press, 2000

[2] , P. Coles, F. Lucchin, *Cosmology: The Origin and Evolution of Cosmic Structure*, Second Edition, John Wiley & Sons, Ltd, 2002

[3] M. Ballardini, *Cosmological Contraints on Cosmic Inflation and Scalar-Tensor Dark Energy Models from CMB Anisotropies and Galaxy Clustering*, Dottorato di ricerca in Astronomia, Universitá di Bologna, 2016

[4] D. Baumann, *Cosmology, Part III: Mathematical Tripos*, dbaumann@damtp.cam.ac.uk

[5] A. Challinor and H. Peiris, *Lecture notes on the physics of cosmic microwave background anisotropies*, AIP Conf. Proc. **1132** (2009) 86 doi:10.1063/1.3151849 [arXiv:0903.5158 [astro-ph.CO]].

[6] Mr. Bayes and Mr. Price. *An Essay towards solving a Problem in the Doctrine of Chances. By the late Rev.Mr. Bayes, communicated by Mr. Price, in a letter to John Canton, M. A. and F. R. S.*, Philosophical Transactions, 53:370418, 1763.

[7] Brunero Liseo, *Introduzione alla statistica bayesiana Settembre*, Springer 2008

[8] A. C. Hall and A. Challinor, *Probing the neutrino mass hierarchy with CMB weak lensing*, Mon. Not. Roy. Astron. Soc. **425** (2012) 1170 doi:10.1111/j.1365-2966.2012.21493.x [arXiv:1205.6172 [astro-ph.CO]].

[9] L. Verde, *Statistical methods in cosmology* Lect. Notes Phys. **800** (2010) 147 doi:10.1007/978-3-642-10598-2_4, [arXiv:0911.3105 [astro-ph.CO]], 2010

[10] R. A. Fisher, *A mathematical examination of the methods of determining the accuracy of an observation by the mean error and by the mean square error*, Monthly Notices of R.A.S. vol. 80, pp. 758770, 1920

[11] Alan Heavens, *Bayesian Statistics in Cosmology*, Institute for Astronomy, University of Edinburgh, Blackford Hill, Edinburgh EH9 3HJ, afh@roe.ac.uk, Lectures and workshops at SCMA V, Penn State, June 2011

[12] L. Perotto, J. Lesgourgues, S. Hannestad, H. Tu and Y. Y. Y. Wong, *Probing cosmological parameters with the CMB: Forecasts from full Monte Carlo simulations*, JCAP **0610** (2006) 013, doi:10.1088/1475-7516/2006/10/013, [astro-ph/0606227], 2006

[13] Euclid mission, *Mapping the geometry of the dark Universe*, Definition Study Report, ESA/SRE(2011)12, July 2011, September 2011 (Revision 1)

[14] Antony Lewis, *CAMB Notes*, http://cosmologist.info, DAMTP, CITA, IoA, Sussex, 2014

[15] F. Finelli *et al.* [CORE Collaboration], *Exploring Cosmic Origins with CORE: Inflation*, arXiv:1612.08270 [astro-ph.CO], 2016

[16] L. Knox, *Determination of inflationary observables by cosmic microwave background anisotropy experiments*, Phys. Rev. D **52** (1995) 4307 doi:10.1103/PhysRevD.52.4307 [astro-ph/9504054].

[17] N. Aghanim *et al.* [Planck Collaboration], *Planck intermediate results. XLVI. Reduction of large-scale systematic effects in HFI polarization maps and estimation of the reionization optical depth*, Astron. Astrophys. **596** (2016) A107, doi:10.1051/0004-6361/201628890, [arXiv:1605.02985 [astro-ph.CO]].

[18] W. Hu and T. Okamoto, *Mass reconstruction with cmb polarization*, Astrophys. J. **574** (2002) 566 doi:10.1086/341110 [astro-ph/0111606].

[19] J. Errard, S. M. Feeney, H. V. Peiris and A. H. Jaffe, *Robust forecasts on fundamental physics from the foreground-obscured, gravitationally-lensed CMB polarization*, JCAP **1603** (2016) no.03, 052 doi:10.1088/1475-7516/2016/03/052 [arXiv:1509.06770 [astro-ph.CO]], 2016

[20] K. M. Smith, D. Hanson, M. LoVerde, C. M. Hirata and O. Zahn, *Delensing CMB Polarization with External Datasets*, JCAP **1206** (2012) 014, doi:10.1088/1475-7516/2012/06/014 [arXiv:1010.0048 [astro-ph.CO]], 2012

[21] M. Ballardini, F. Finelli, C. Fedeli and L. Moscardini, *Probing primordial features with future galaxy surveys*, JCAP **1610** (2016) 041, doi:10.1088/1475-7516/2016/10/041 [arXiv:1606.03747 [astro-ph.CO]], 2016

[22] C. Alcock and B. Paczynski, *An evolution free test for non-zero cosmological constant*, Nature 281, pag. 358, 1979

[23] L. R. Abramo, *The full Fisher matrix for galaxy surveys*, Mon. Not. Roy. Astron. Soc. **420** (2012) 3, doi:10.1111/j.1365-2966.2011.20166.x [arXiv:1108.5449 [astro-ph.CO]], 2012

[24] L. Pozzetti *et al.*, *Modelling the number density of H emitters for future spectroscopic near-IR space missions*, Astron. Astrophys. **590** (2016) A3, doi:10.1051/0004-6361/201527081 [arXiv:1603.01453 [astro-ph.GA]], 2016

[25] P. A. R. Ade *et al.* [Planck Collaboration], *Planck 2015 results. XX. Constraints on inflation*, Astron. Astrophys. **594** (2016) A20, doi:10.1051/0004-6361/201525898, [arXiv:1502.02114 [astro-ph.CO]].

[26] P. A. R. Ade *et al.* [Planck Collaboration], *Planck 2015 results. XIII. Cosmological parameters*, Astron. Astrophys. **594** (2016) A13, doi:10.1051/0004-6361/201525830 [arXiv:1502.01589 [astro-ph.CO]].

[27] T. Kajita, *Nobel Lecture: Discovery of atmospheric neutrino oscillations*, Reviews of Modern Physics, doi:10.1103/RevModPhys.88.030501, 2016, http://adsabs.harvard.edu/abs/2016RvMP...88c0501K

[28] A. B. McDonald, *Nobel Lecture: The Sudbury Neutrino Observatory: Observation of flavor change for solar neutrinos*, Reviews of Modern Physics, doi:10.1103/RevModPhys.88.030502, 2016, http://adsabs.harvard.edu/abs/2016RvMP...88c0502M

[29] G. Mangano, G. Miele, S. Pastor and M. Peloso, *A Precision calculation of the effective number of cosmological neutrinos*, Phys. Lett. B **534** (2002) 8, doi:10.1016/S0370-2693(02)01622-2 [astro-ph/0111408].

[30] K. N. Abazajian *et al.*, *Light Sterile Neutrinos: A White Paper*, arXiv:1204.5379 [hep-ph].

[31] J. Hasenkamp and J. Kersten, *Dark radiation from particle decay: cosmological constraints and opportunities*, JCAP **1308** (2013) 024, doi:10.1088/1475-7516/2013/08/024 [arXiv:1212.4160 [hep-ph]].

[32] M. Gerbino, K. Freese, S. Vagnozzi, M. Lattanzi, O. Mena, E. Giusarma and S. Ho, *Impact of neutrino properties on the estimation of inflationary parameters from current and future observations*, arXiv:1610.08830 [astro-ph.CO].

[33] E. Di Valentino *et al.* [CORE Collaboration], *Exploring Cosmic Origins with CORE: Cosmological Parameters*, arXiv:1612.00021 [astro-ph.CO].

[34] M. Kleban and M. Schillo, *Spatial Curvature Falsifies Eternal Inflation*, JCAP **1206** (2012) 029 doi:10.1088/1475-7516/2012/06/029 [arXiv:1202.5037 [astro-ph.CO]].

[35] A. H. Guth and Y. Nomura, *What can the observation of nonzero curvature tell us?*, Phys. Rev. D **86** (2012) 023534 doi:10.1103/PhysRevD.86.023534 [arXiv:1203.6876 [hep-th]].

[36] F. Finelli *et al.* [CORE Collaboration], *Exploring Cosmic Origins with CORE: Inflation*, arXiv:1612.08270 [astro-ph.CO].

[37] A. Kosowsky and M. S. Turner, *CBR anisotropy and the running of the scalar spectral index*, Phys. Rev. D **52** (1995) R1739 doi:10.1103/PhysRevD.52.R1739 [astro-ph/9504071].

[38] M. Archidiacono, T. Brinckmann, J. Lesgourgues and V. Poulin, *Physical effects involved in the measurements of neutrino masses with future cosmological data*, arXiv:1610.09852 [astro-ph.CO].

[39] J. Errard, S. M. Feeney, H. V. Peiris and A. H. Jaffe, *Robust forecasts on fundamental physics from the foreground-obscured, gravitationally-lensed CMB polarization*, JCAP **1603** (2016) no.03, 052 doi:10.1088/1475-7516/2016/03/052 [arXiv:1509.06770 [astro-ph.CO]].

[40] L. Wolz, M. Kilbinger, J. Weller and T. Giannantonio, *On the Validity of Cosmological Fisher Matrix Forecasts*, JCAP **1209** (2012) 009 doi:10.1088/1475-7516/2012/09/009 [arXiv:1205.3984 [astro-ph.CO]].

[41] C. D. Leonard, P. Bull and R. Allison, *Spatial curvature endgame: Reaching the limit of curvature determination*, Phys. Rev. D **94** (2016) no.2, 023502 doi:10.1103/PhysRevD.94.023502 [arXiv:1604.01410 [astro-ph.CO]].

[42] J. B. Muoz, E. D. Kovetz, A. Raccanelli, M. Kamionkowski and J. Silk, *Towards a measurement of the spectral runnings*, arXiv:1611.05883 [astro-ph.CO].

[43] R. Allison, P. Caucal, E. Calabrese, J. Dunkley and T. Louis, *Towards a cosmological neutrino mass detection*, Phys. Rev. D **92** (2015) no.12, 123535 doi:10.1103/PhysRevD.92.123535 [arXiv:1509.07471 [astro-ph.CO]].